Cell Reports

Article

Spike-specific IgG4 generated post BNT162b2 mRNA vaccination is inhibitory when directly competing with functional IgG subclasses

Graphical abstract

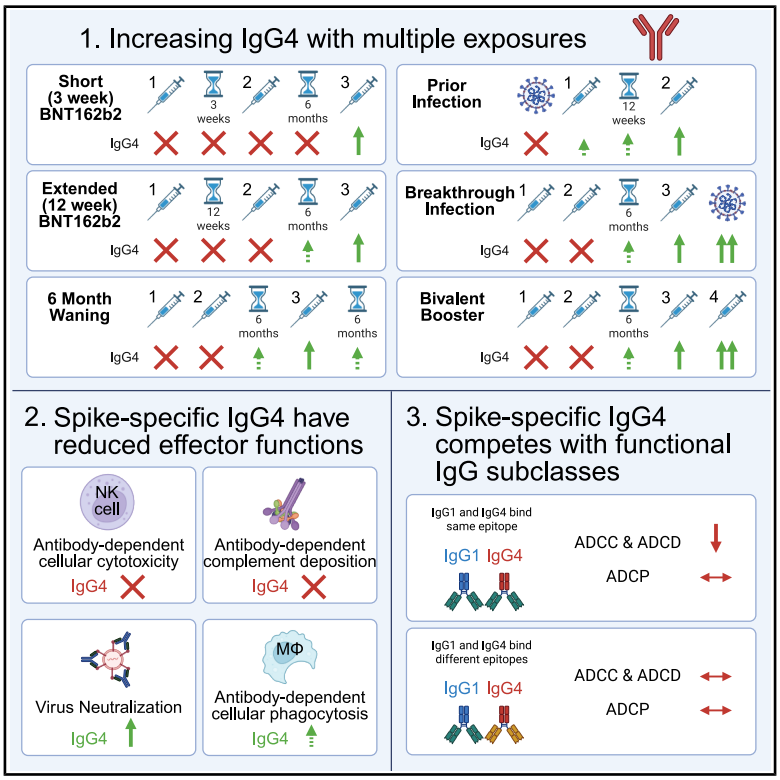

Highlights

- Spike-specific IgG4 is impacted by vaccine interval and boosting and hybrid immunity
- Spike-specific IgG4 have reduced ADCC, ADCP, and ADCD activity
- IgG4 competes the ADCC activity of IgG1 when binding to overlapping epitopes

Authors

Jerry C.H. Tam, Abbie C. Sibayan, Jeffrey Seow, ..., Blair Merrick, Richard J. Stanton, Katie J. Doores

Correspondence

katie.doores@kcl.ac.uk

In brief

Tam et al. identified SARS-CoV-2 exposure histories that favor development of Spike-specific IgG4 responses. Although IgG4 monoclonal antibodies have reduced effector-function activity, in the context of a polyclonal response, IgG4 is only inhibitory when directly competing with functional antibody subclasses that bind overlapping epitopes.

Tam et al., 2025, Cell Reports *44*, 116000
July 22, 2025
https://doi.org/10.1016/j.celrep.2025.116000

CellPress

Cell Reports

CellPress
OPEN ACCESS

Article

Spike-specific IgG4 generated post BNT162b2 mRNA vaccination is inhibitory when directly competing with functional IgG subclasses

Jerry C.H. Tam,[1] Abbie C. Sibayan,[1] Jeffrey Seow,[1] Carl Graham,[1] Ashwini Kurshan,[1] Blair Merrick,[2] Richard J. Stanton,[3] and Katie J. Doores[1,4,*]

[1]Department of Infectious Diseases, School of Immunology & Microbial Sciences, King's College London, London, UK
[2]Centre for Clinical Infection and Diagnostics Research, Department of Infectious Diseases, Guy's and St Thomas' NHS Foundation Trust, London, UK
[3]Division of Infection and Immunity, School of Medicine, Cardiff University, Cardiff, UK
[4]Lead contact
*Correspondence: katie.doores@kcl.ac.uk
https://doi.org/10.1016/j.celrep.2025.116000

SUMMARY

COVID-19 vaccines proved vital in controlling the SARS-CoV-2 pandemic. Both neutralizing and effector-function activities of Spike-specific antibodies are important for their protective activity. Several studies have reported that COVID-19 mRNA vaccines can lead to elevated levels of Spike-specific immunoglobulin G4 (IgG4), an anti-inflammatory subclass with reduced binding to Fcγ receptors. We show that Spike-specific IgG4 levels following BNT162b2 vaccination are impacted by the interval between and frequency of vaccine boosts, prior or post SARS-CoV-2 infection and bivalent vaccine boosters. Through expression of IgG1, IgG2, IgG3, and IgG4 subclasses of SARS-CoV-2 antibodies, we demonstrate that while IgG4 has reduced effector-function activity, including antibody-dependent cellular cytotoxicity (ADCC), antibody-dependent complement deposition (ADCD), and antibody-dependent cellular phagocytosis, IgG4 is only inhibitory when directly competing with functional IgG subclasses binding to overlapping epitopes. ADCC and ADCD activity in plasma was not depleted by adding a cocktail of Spike-specific IgG4 monoclonal antibodies, suggesting that the non-stimulatory effect of Spike-specific IgG4 may be hidden in polyclonal mixes.

INTRODUCTION

The COVID-19 pandemic led to the rapid development and deployment of several COVID-19 vaccines utilizing a range of different vaccine platforms.[1] Vaccines targeting SARS-CoV-2 Wuhan Spike glycoprotein have been highly effective in reducing morbidity and mortality from COVID-19.[2] In particular, the pandemic led to the first widespread clinical use of mRNA-based vaccines; including BNT162b2 from BioNTech/Pfizer[3] and Spikevax from Moderna.[4] These were initially deployed in a two-dose regimen, separated by a 3-week interval.[3,4] However, the United Kingdom quickly changed to a 12-week interval between doses, with the rationale of ensuring some degree of SARS-CoV-2 immunity for a wider proportion of the population.[5] To overcome waning antibody levels,[6] a third dose was offered as a booster, which had the additional benefit of broadening the antibody response toward SARS-CoV-2 variants of concern[7–10] as well as leading to an increased antibody-binding avidity.[7] More recently, updated mRNA vaccines based upon newer variants such as BA.1 and XBB.1.5 have been used as boosters,[11] not only for individuals primed with COVID-19 Wuhan-1 mRNA vaccines[11,12] but also for individuals who had initially received other vaccine types, such as the AstraZeneca chimpanzee adenovirus vector (ChAdOx) COVID-19 vaccine, AZD1222.[13] Given the safety and efficacy of COVID-19 mRNA vaccines, there has been increased interest in using this vaccine platform for more applications, including vaccines against other pathogenic viruses as well as against bacteria, and as immunotherapies for cancer treatment.[14]

While antibody binding and neutralization correlate with protection against SARS-CoV-2 infection and severe COVID-19 disease,[15] the Fc region can also collaborate to enhance the protective capacity of antibodies. Animal studies have shown the importance of Fc-mediated effector functions of monoclonal antibodies (mAbs) for limiting SARS-CoV-2 immunopathology and viral persistence.[16–19] Furthermore, robust antibody Fc effector functions induced by vaccines correlate with protection in animal challenge studies.[20–22]

It has previously been reported that the use of COVID-19 mRNA-based vaccines can lead to skewing of the immunoglobulin G (IgG) subclass usage against SARS-CoV-2 Spike.[13,23–25] In addition to the majority IgG1 and IgG3 response, Spike-specific IgG4 could also be detected at low levels in some individuals around 6–7 months after a second dose of either BNT162b2 or Spikevax[13,25] and at higher levels in the majority of individuals following a third dose of BNT162b2, as well as

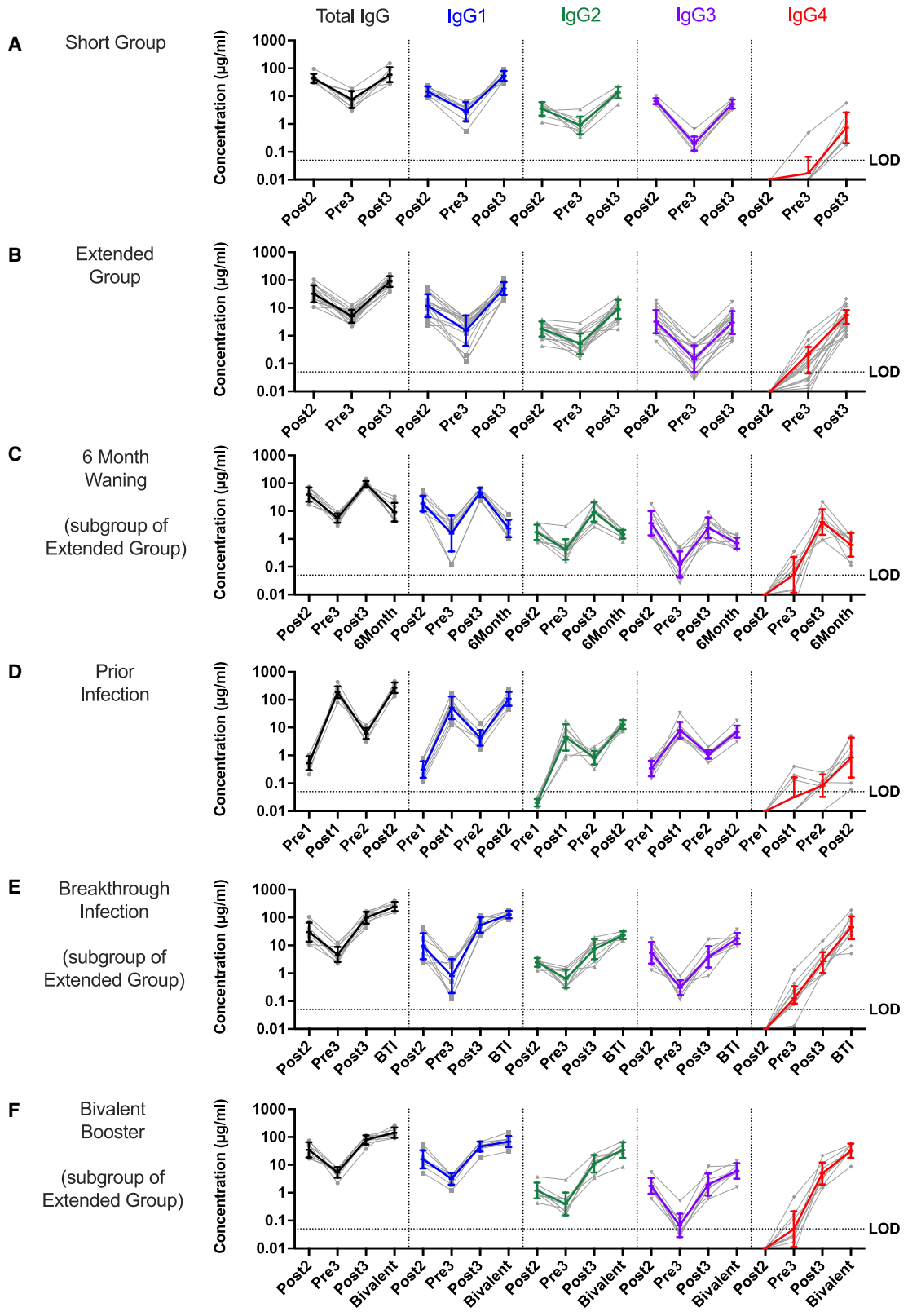

(legend on next page)

following a BNT162b2 booster vaccine in individuals who initially received the AZD1222 vaccine.[13] This increase in Spike-specific IgG4 is notable, given that IgG4 is usually thought to be anti-inflammatory[26] and is not typically observed following vaccination or infection.[27] Instead, antigen-specific IgG4 has been reported in the context of allergy,[28] autoimmunity,[29,30] and chronic inflammatory conditions.[31] The perceived role of IgG4 as anti-inflammatory comes from its reduced ability to stimulate Fc-mediated antibody effector functions,[26,32] including antibody-dependent cellular cytotoxicity (ADCC), antibody-dependent complement deposition (ADCD), and antibody-dependent cellular phagocytosis (ADCP), due to the reduced affinity of the IgG4 Fc domain for FcγR receptors, in particular FcγRIIA, FcγRIIIA, and FcγRIIIB.[33] IgG4 is the only immunoglobulin that can undergo Fab-arm exchange, a process in which half-molecules of IgG4 combine randomly, resulting in bispecific immunoglobulins with reduced binding and/or neutralizing activity due to a lower valency of binding.[34]

Antibody effector functions are important in clearing infection through binding of antibodies to antigens expressed on the surface of infected cells or to free virus.[35] Effector functions have been shown to be important in both prophylactic and therapeutic protection models.[20,36] For example, introduction of the LALA-PG mutations (L234A + L235A + P329G), which are known to reduce the binding of IgGs to FcγRs, reduces the therapeutic activity of neutralizing antibodies against SARS-CoV-2.[37] Furthermore, non-neutralizing Spike-specific IgG1 can confer protection in small-animal challenge models if passively administered prior to challenge.[38] While the relevance of IgG subclass has not been studied *in vivo* in the context of SARS-CoV-2 infection, antibody passive transfer experiments in the context of influenza virus infection have revealed that the IgG subclass is important in determining protection.[39,40] However, animal studies have limited utility for understanding the impact of increased levels of antigen-specific IgG4 given that it is only found in humans and great apes.[41]

While several studies report elevated levels of Spike-specific IgG4 following mRNA vaccination,[13,23–25] there is an incomplete knowledge of factors that might influence the switch to IgG4 and how the level of Spike-specific IgG4 might be impacted by further mRNA vaccine booster doses and/or breakthrough infection (BTI). Furthermore, there is an incomplete understanding of the functional implications of the presence of Spike-specific IgG4 on the functional activity of the Spike-specific total IgG. Here, we investigated the impact of (1) mRNA vaccine interval and frequency, (2) hybrid immunity (including infection pre-vaccination and BTI), (3) bivalent vaccines, and (4) time from SARS-CoV-2 infection in unvaccinated individuals on the amount of IgG4 produced, the IgG4 binding specificity, breadth, and avidity, and the effector-function activity in immune plasma. We observed that IgG4 production was impacted by the number of mRNA doses, the interval between these doses, and SARS-CoV-2 infection (both pre- and post vaccination). Through generation of a panel of class-switched Spike-specific mAbs, including IgG1, IgG2, IgG3, and IgG4, we demonstrate that while IgG4 poorly activates ADCC, ADCP, and ADCD, it is capable of potent and equivalent neutralization as IgG1. Importantly, IgG4 is only anti-inflammatory when competing directly for binding with an activating IgG1 but is functionally silent if not competing. These findings provide important insights into the functional implications of elevated levels of Spike-specific IgG4 following BNT162b2 mRNA vaccination.

RESULTS

Spike-specific IgG4 class switching increases with multiple BNT162b2 vaccine exposures and time

To gain further understanding of the factors influencing class switching to Spike-specific IgG4 during mRNA vaccination, we studied selected plasma from several United Kingdom (UK)-based vaccine cohorts (Table S1A and Figure S1A). These groups differed in (1) the spacing between the first and second vaccine doses, (2) prior or subsequent SARS-CoV-2 infection, and (3) use of a bivalent booster vaccine based on Wuhan-1/BA.1. We first measured the concentration of SARS-CoV-2 Spike-specific IgG in a subclass-specific manner for each group using a semiquantitative ELISA (Figure 1).

Following the standard BNT162b2 vaccination protocol (i.e., a 3- to 4-week interval between first and second dose, here referred to as "short group"), total IgG levels averaged 45.1 μg/mL after two mRNA doses (Figure 1A). As previously reported, the total Spike-specific IgG levels waned over time, such that at 6 months post vaccination they decreased to 9.05 μg/mL. A third vaccine dose was able to increase the level back to 67.0 μg/mL. This pattern of IgG levels can largely be explained by changes in IgG1, IgG2, and IgG3, which all follow a similar pattern. However, Spike-specific IgG4 only became detectable after the third dose of vaccine, similar to observations previously reported,[24,25] with levels reaching 1.47 μg/mL.

In the UK, the majority of individuals receiving the BNT162b2 vaccine did so with an extended 8- to 12-week interval between the first and second doses (referred to here as "extended group"). The trends in total IgG, IgG1, IgG2, and IgG3 levels were similar to that of the short group (Figure 1B). However, in contrast to the short group, Spike-specific IgG4 could be observed earlier, with Spike-specific IgG4 being detected in

Figure 1. Spike-specific IgG4 production in individuals with different exposure histories

Semiquantitative ELISA measurement of wild-type (WT) SARS-CoV-2 Spike-specific total IgG (black), IgG1 (blue), IgG2 (green), IgG3 (purple), and IgG4 (red) for plasma at (A) 3-week interval between first- and second-dose group (short group, $n = 8$), (B) 12-week interval between first- and second-dose group (extended group, $n = 17$), (C) subgroup of extended group with sample at 6 months post third dose ($n = 9$), (D) prior infection group ($n = 8$), (E) subgroup of extended group with a breakthrough infection after three doses ($n = 9$), and (F) subgroup of extended group with a bivalent WT/BA.1 booster 1 year after third dose ($n = 8$). Samples paired from individuals in gray with colored data representing geometric mean ± SD (standard deviation). Pre1, before first dose; Post1, 3 weeks after first dose; Pre2, before second dose; Post2, 3 weeks after second dose; Pre3, before third dose; Post3, 3 weeks after third dose; 6Month, 6 months after third dose; BTI, 3 weeks after breakthrough infection; Bivalent, 3 weeks after bivalent dose. See Table S1 for demographics and Figure S1 for precise timings. Semiquantitative ELISA limit of detection (LOD) is 0.05 μg/mL and is shown by the horizontal dotted line. See also Table S1 and Figure S1.

the majority of individuals at 6 months post second dose and prior to the third vaccination, suggesting that the vaccine interval can influence class switching to IgG4. Interestingly, unlike at 6 months after the second vaccine dose when IgG1 responses had waned, IgG4 responses had increased. However, at 6 months after the third vaccine dose, all IgG subclasses had waned, including IgG4 (Figure 1C).

Next, we examined the impact of hybrid immunity on IgG4 production, including infection prior to vaccination as well as a BTI post vaccination. A more heterogeneous response was observed in individuals who had SARS-CoV-2 infection prior to vaccination, with three out of eight volunteers producing Spike-specific IgG4 after the first vaccine dose and all producing Spike-specific IgG4 after two doses (Figure 1D). A BTI after three BNT162b2 vaccinations lead to a further increase in Spike-specific IgG4, reaching levels of only ~5-fold below Spike-specific IgG1 in some individuals (Figure 1E). Some individuals were subsequently vaccinated a fourth time with a bivalent wild-type (WT)/BA.1 mRNA vaccine, and this additional vaccination led to a further increase in Spike-specific IgG4 levels as well as in total IgG, IgG1, IgG2, and IgG3 levels (Figure 1F).

Together, these data demonstrate that Spike-specific IgG4 generated in response to mRNA vaccination is impacted by the interval and number of vaccinations, the time since vaccination, and an infection prior to or after BNT162b2 vaccination.

Spike-specific IgG4 is not detected in a longitudinal infection cohort

Several studies have reported a continued evolution of the antibody response post SARS-CoV-2 infection as demonstrated by increased somatic hypermutation of Spike-specific mAbs isolated at 6 months post infection.[42] To determine whether time from infection might influence the production of Spike- and/or nucleocapsid-specific IgG4 post infection, we measured total IgG and IgG4 levels in a longitudinal infection cohort from wave 1 (i.e., beginning March 2020) that was followed until 33 weeks post infection (Table S1B and Figure S1B). Spike-specific IgG4 was at or below the limit of detection in sera from individuals experiencing mild (Figure 2A) or severe (Figure 2B) disease, even up to similar times post-infection as for the post-vaccination volunteers. These data suggest that the production of Spike-specific IgG4 is not a feature inherent to the Spike protein itself or the time post SARS-CoV-2 Spike exposure, and that multiple exposures are important.

IgG4 class switch is Spike specific

As the levels of Spike-specific IgG4 were boosted upon BTI, we next determined whether IgG4 production was restricted to Spike or if IgG4 to nucleocapsid (which is not present in the BNT162b2 vaccine) could be detected following BTI. After two BTIs post vaccination, there was a robust Spike-specific IgG4 response, which persisted for at least 6 months after the second infection (Figure 2C). However, there was no nucleocapsid-specific IgG4 detected, even 6 months after a second BTI.

Some individuals also received an influenza vaccine at the same time as their third BNT162b2 vaccination. We therefore investigated whether the immune environment generated in response to the mRNA vaccination might impact on IgG4 class switching to influenza hemagglutinin (HA). No HA-specific IgG4 was detected in any of these plasma samples (Figure 2D). Combined, these data indicate that the class switching to IgG4 is specific for SARS-CoV-2 Spike in the context of mRNA vaccination.

Spike-specific IgG4 is distributed across RBD and NTD domains

We next investigated the domains on SARS-CoV-2 Spike targeted by the IgG4 response with a focus on the extended group. The two major Spike domains targeted by neutralizing antibodies are the receptor-binding domain (RBD), which interacts with the host cell receptor angiotensin converting enzyme 2 (ACE2),[43] and the N-terminal domain (NTD), whose function is less well defined.[44] Binding of IgG4 to both RBD and NTD could be detected by ELISA (Figure 2E). When considering the proportion of IgG4 binding to each domain, 33.6% of the Spike-specific IgG4 was targeted against RBD, similar to 30.2% (standard deviation [SD] 4.53) of the total IgG, while 19.7% (SD 9.87) of the Spike-specific IgG4 was targeted against NTD, similar to 23.8% of the total IgG (Figure 2F), suggesting that the Spike-specific IgG4 response is not skewed toward a specific Spike domain.

Spike-specific IgG4 has variant binding breadth similar to that of total Spike-specific IgG

Previous studies have shown that repeated COVID-19 vaccination can lead to increased antibody binding and neutralization breadth against newer SARS-CoV-2 variants of concern.[7,45,46] Given that Spike-specific IgG4 also emerges and increases following multiple mRNA vaccinations, we therefore measured the breadth of the Spike-specific IgG1 and IgG4 responses by measuring variant Spike-binding breadth by ELISA. We focused on the Spike-specific total IgG and IgG4 in the extended group following three BNT162b2 doses (Figure 2G). Similar to the total IgG binding, comparable levels of IgG4 binding were observed against the WT, Beta, Delta, and BA.1 SARS-CoV-2 recombinant Spikes.

Spike-specific IgG4 has a delayed avidity increase

Antibody avidity can also be enhanced by repeated antigen exposure, either through vaccination or infection.[7,45] Previous studies have associated the increased Spike-specific total IgG avidity with increasing levels of IgG4.[25] However, this study did not specifically measure avidity changes for Spike-specific IgG1 and IgG4 independently. Here, we first measured the avidity index against WT Spike of the total IgG by comparing the area under the curve in ELISA, with and without an 8 M urea washing step.[7] Similar to previously published results,[7] the avidity of Spike-specific total IgG increased with additional vaccine doses as well as time post vaccination, up until the third dose when the avidity score reached a plateau (Figure 2H and Table S2). When considering the avidity of Spike-specific IgG1 and IgG4 independently, the IgG1 avidity mirrored the increasing avidity pattern observed for the total IgG (Figure 2I). In contrast, the avidity of Spike-specific IgG4 when first detected at 6 months post second vaccine (Pre3) was low (35.0%, SD 7.62) compared to the total IgG (73.4%, SD 5.62) and to IgG1 (72.2%, SD 6.32) (Figure 2I).

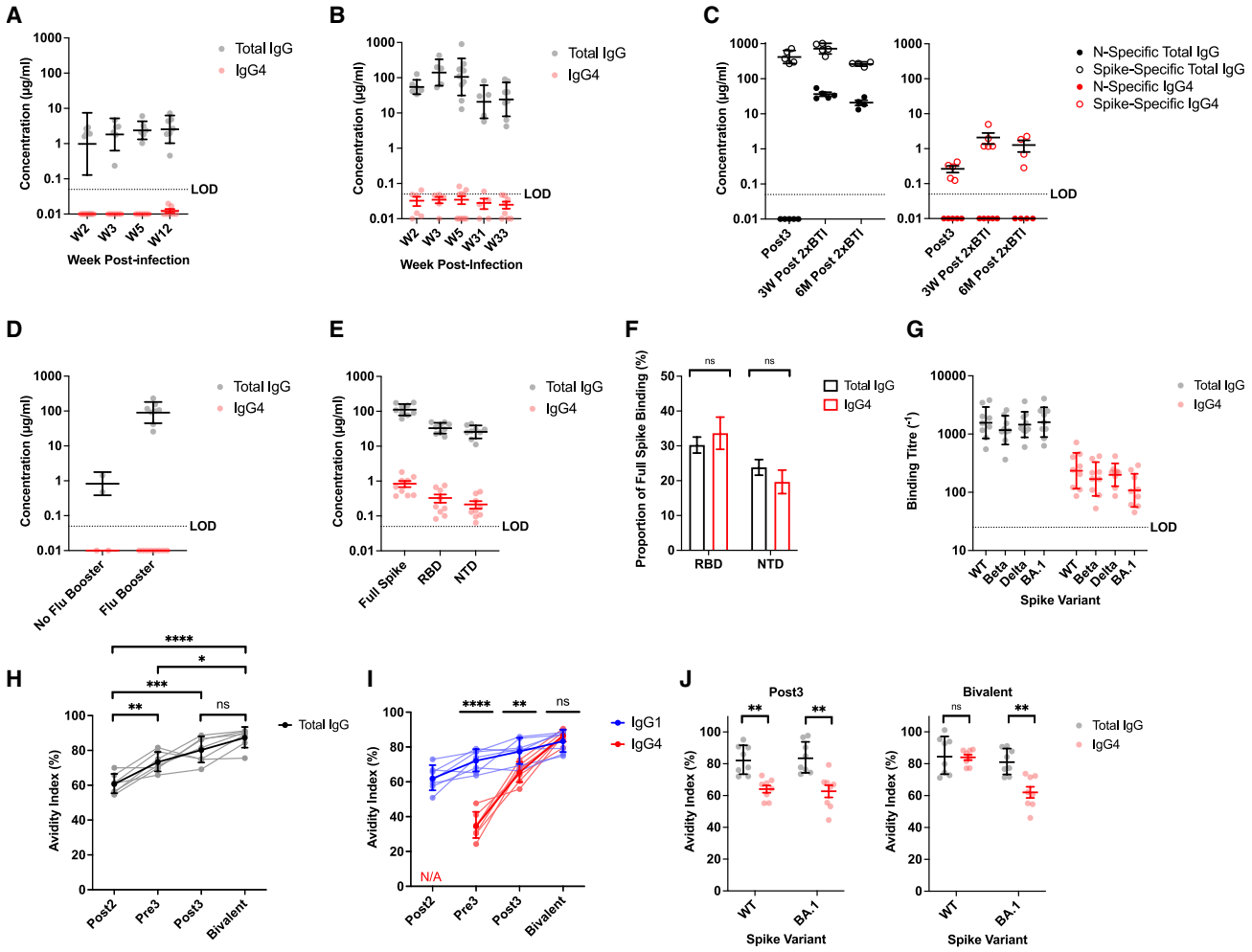

Figure 2. Specificity and avidity of IgG4 arising from BNT162b2 mRNA vaccination

(A and B) Concentration of Spike-specific total IgG (black/gray) and IgG4 (red/pink) in sera for (A) a mild infection group and (B) severe, ITU admission infection group. The horizontal dotted line shows the lower limit of detection (LOD, 0.05 μg/mL) for IgG and IgG4.

(C) Concentration of SARS-CoV-2 N-specific total IgG (filled black circles), Spike-specific total IgG (clear black circles), N-specific IgG4 (filled red circles), and Spike-specific IgG4 (clear red circles) 3 weeks after third dose (Post3), 3 weeks after second breakthrough infection (3W Post 2xBTI), and 6 months after second breakthrough infection (6M Post 2xBTI).

(D) Concentration of hemagglutinin-specific total IgG (black/gray) or IgG4 (red/pink) with or without influenza booster given with third dose to extended group.

(E) ELISA measurement of total IgG (black/gray) and IgG4 (red/pink) targeted against WT SARS-CoV-2 full Spike, receptor-binding domain (RBD), and N-terminal domain (NTD) in extended group Post3 samples.

(F) RBD and NTD binding total IgG (black) and IgG4 (red) as a proportion of binding to full Spike.

(G) Total IgG (black/gray) and IgG4 (red/pink) binding to WT, Beta, Delta, and BA.1 Spike in extended group Post3 samples.

(H) Serum antibody avidity of total IgG (black) binding to WT Spike in Post2, Pre3, Post3, and bivalent samples from the bivalent group.

(I) As in (H), but for IgG1 (blue) and IgG4 (red). Significance values shown between IgG1 and IgG4 avidity for the same sample time point.

(J) Serum antibody avidity of total IgG (black/gray) and IgG4 (red/pink) against WT and BA.1 recombinant Spikes for Post3 and bivalent samples from the bivalent group.

In all panels, samples paired from an individual are in lighter color, with darker-colored data representing geometric mean ± SD. Data representative of three technical replicates. ns, not significant; $^{*}p < 0.05$, $^{**}p < 0.01$, $^{***}p < 0.001$, $^{****}p < 0.0001$, paired t tests (F, I, and J) and multiple-comparisons repeated-measures ANOVA (H) calculated using GraphPad Prism. See also Tables S2 and S3.

However, the IgG4 avidity increased following a third BNT162b2 (Post3, 65.3%, SD 5.84), with a smaller increase following a subsequent bivalent booster (86.4%, SD 3.44) to reach similar avidity levels to the Spike-specific IgG1 (83.4%, SD 6.23). Although the avidity against WT Spike became equal after a bivalent booster, the avidity against the BA.1 Spike remained lower for IgG4 (62.0%, SD 9.96) compared to the total IgG (81.4%, SD 8.13) (Figure 2J and Table S3), suggesting that affinity maturation of IgG4 against the BA.1 Spike is less. Overall, the avidity of Spike-specific IgG4 was delayed compared to IgG1 but plateaued at a similar level after three vaccine doses against the matched vaccine antigen.

Serum antibody functional activity is associated with IgG1 levels but not IgG4 levels

We next investigated the functional effect of the increase in Spike-specific IgG4 on functional activity of polyclonal plasma, including neutralization, ADCC, ADCP, and complement deposition. Given the largest increase in Spike-specific IgG4 was observed between the second and third dose of BNT162b2 vaccine, we investigated the differences in functional activity between plasma from these time points (Post2 and Post3) in the extended group and the bivalent booster group. Neutralization activity is largely antibody Fc binding independent,[47] and, as previously shown, there was a trend toward increasing plasma neutralizing activity between the second and third dose of mRNA vaccine against WT (although this did not reach significance), consistent with the increase in Spike-specific total IgG (Figure 3A).[7] Both the IgG1 and IgG4 levels Post2, Post3, and post bivalent mRNA vaccines correlated with the ID_{50} values (Figure 3C).

ADCC is dependent on CD16 expressed on natural killer (NK) cells, so we tested the ability of the plasma to stimulate an NK-92 cell line expressing CD16 to degranulate using CD107a expression as the readout (Figure S2).[48,49] In our assay, there was no significant difference in NK cell degranulation between the second and third dose of mRNA vaccine at the highest dilution tested (1:50) (Figure 3D), although there was notable heterogeneity between whether ADCC increased or decreased, presumably due to the differing IgG1 and IgG4 levels. We therefore correlated the level of NK cell degranulation with concentration of Spike-specific IgG1 and IgG4. NK cell degranulation positively correlated with Spike-specific IgG1 (Figure 3F), IgG2, and IgG3 (Figure S3A), but no significant correlations were observed with Spike-specific IgG4 levels (Figure 3F) or between the ratio of IgG1 to IgG4 (Figure S3B). In the cohort receiving the bivalent vaccine, the additional WT/BA.1 mRNA vaccination had no impact on ADCC activity despite small increases in Spike-specific IgG4 levels, suggesting a homeostatic limit to the amount of ADCC (Figure 3E).

Next, we compared the ability of plasma collected following second and third doses of BNT162b2 vaccine to stimulate ADCD and ADCP. As ADCD requires a complement source lacking antibodies to the SARS-CoV-2 Spike, we utilized guinea pig complement serum that was naive to SARS-CoV-2 Spike.[50] Comparing ADCD activity in plasma post second and third doses showed a 3.0-fold increase in the level of complement deposition (Figure 3G). There was a positive correlation between ADCD activity and IgG1 level, but no significant correlation was observed with IgG4 (Figure 3I). ADCP activity was measured using THP-1 cells as the effector cells and fluorescent beads coated with recombinantly expressed SARS-CoV-2 Spike.[51] A 1.8-fold increase in ADCP activity was observed following the third mRNA vaccine (Figure 3J). Similar to ADCD activity, there was a positive correlation between ADCP activity and IgG1 level, but a weak positive correlation was also observed with IgG4 (Figure 3L). Following administration of the bivalent booster, ADCD and ADCP levels remained unchanged, which is consistent with the smaller increase in Spike-specific IgG levels post bivalent booster (Figures 3H and 3K).

A previous study reported a decrease in ADCD and ADCP following a third dose of BNT162b2 mRNA vaccine[25]; however, in these experiments the serum input was normalized to the amount of Spike-specific total IgG at each time point. When the ADCC, ADCD, and ADCP activity measured in our experiments was normalized to the amount of Spike-specific total IgG, we also observed a decrease in ADCD, ADCP, and ADCC for the Post3 samples compared to Post2 samples, suggesting that increasing IgG4 may limit effector-function activity (Figure S3C). No significant difference was observed for neutralization. Nevertheless, given that there are increases in all IgG subclasses between Post2 and Post3 (Figure 1B), the absolute ability of serum to activate these effector functions would be most physiologically relevant, rather than the relative functional ability.

In summary, between the second and third mRNA vaccine doses, where there is a 3.2-fold increase in IgG1 and an ~100-fold increase in IgG4, we observe increased neutralization, ADCD, and ADCP in the plasma of individuals in the extended group. However, despite ADCC activity correlating with IgG1 concentration, ADCC activity in plasma did not increase significantly, suggesting that Spike-specific IgG4 may impact effector-function activities differently.

IgG4 maintains neutralization activity but loses Fc-dependent effector functions

Next, we investigated the specific contribution that IgG4 makes to the effector-function activity measurements. Due to the technical challenges in separating the different subclasses of Spike-specific IgG from plasma, we recombinantly expressed IgG1, IgG2, IgG3, and IgG4 versions of a panel of SARS-CoV-2-specific mAbs previously isolated from infected or vaccinated individuals.[52,53] mAbs were selected based on their ability to activate degranulation of CD16 expressing NK cells in the ADCC assay (Figures S4A and S4B). mAbs selected targeted several different epitopes on Spike.[54] P008_60 is SD1 specific,[52] P008_87 is a class 3 RBD-specific mAb that binds an epitope on the outer face of RBD,[52] VA14_1 and VA14_R39 are class 4 RBD-specific mAbs that bind the interior face of RBD,[53] P008_90 is a class 1/2 RBD-specific mAb,[52] and P008_99 is NTD specific[52] (Figure S4A). Note that none of the class 1 RBD-specific mAbs that bind the ACE2 receptor binding site were able to facilitate ADCC. IgG subclass did not affect the binding to SARS-CoV-2 Spike for any of the mAbs studied (Figure S6).

We first investigated the ability of immune complexes containing the different subclasses of IgG to bind to Fc receptors on the surface of various immune cells. NK cells express CD16 (FcγRIIIa), and incubation of mAb-immune complexes with NK cells demonstrated similar binding of IgG1 and IgG3 antibodies but very low binding of the IgG2 and IgG4 subclasses (Figure S5A). Raji cells expressing CD32 (FcγRIIa and FcγRIIb)[55] bound immune complexes of all subclasses equally (Figure S5B). THP-1 cells differentiated using phorbol myristate acetate (PMA) and interferon-γ express both CD32 (FcγRII) and CD64 (FcγRI),[56] and these showed weaker binding of IgG4 compared with other subclasses (Figure S5C). Given that there was no difference in binding to Raji cells expressing CD32 alone, the difference in binding to the differentiated THP-1 cells is likely due to reduced binding between CD64 and the IgG4 Fc region.

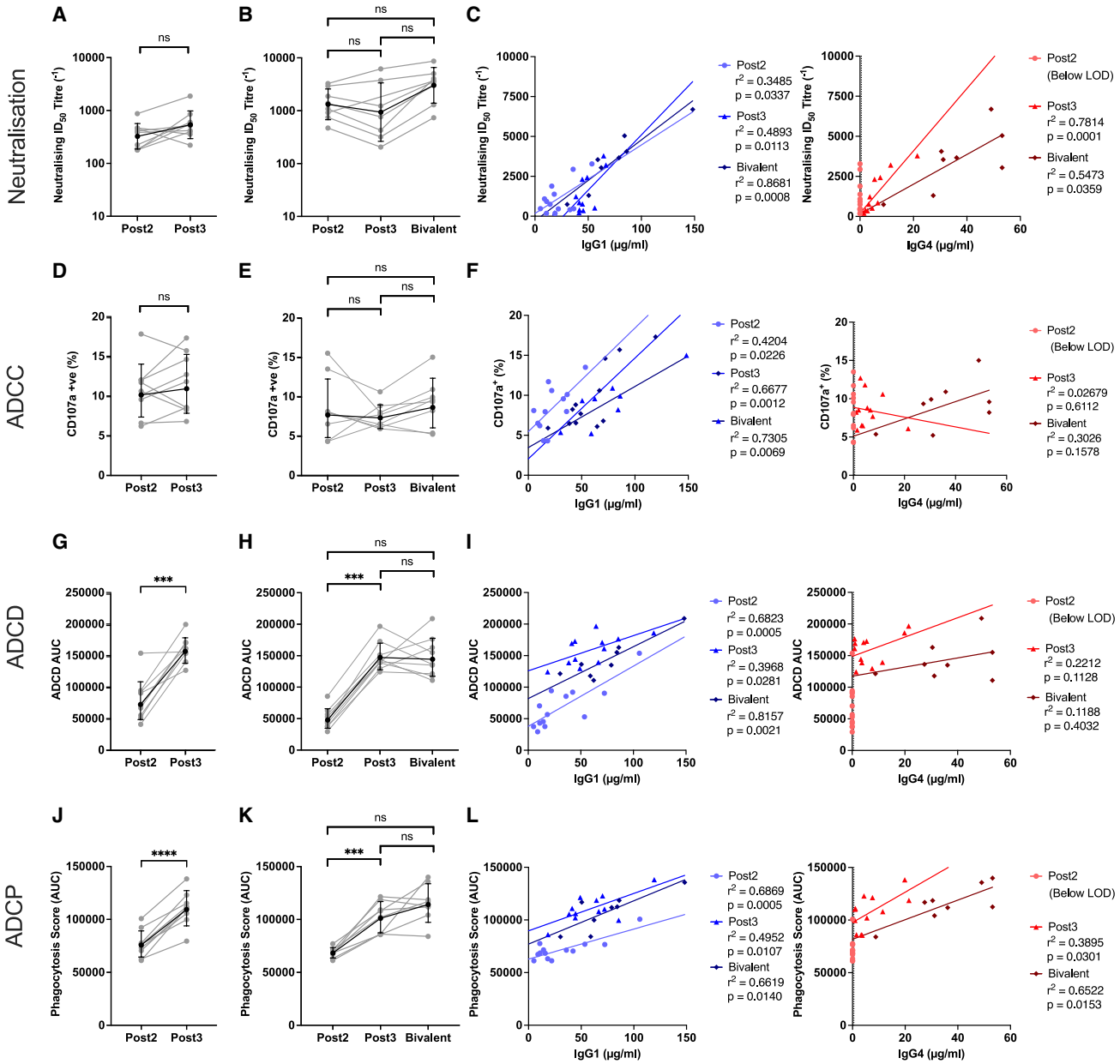

Figure 3. Functional activity of plasma with increasing Spike-specific IgG4

(A) Neutralizing 50% inhibitory dose (ID_{50}) titer against WT SARS-CoV-2 Spike pseudotyped virus for extended group Post2 and Post3 samples.

(B) Neutralizing ID_{50} titer for bivalent group Post2, Post3, and bivalent samples.

(C) Correlation between neutralizing ID_{50} and IgG1 (blue) or IgG4 (red) concentration, with lighter color for Post2, medium color for Post3, and darkest for bivalent.

(D–F) As (A)–(C) but for antibody-dependent cellular cytotoxicity (ADCC) assay, measuring surface CD107a on activated NK cells. A serial dilution of plasma was used, and the percentage CD107a surface expression is shown for a 1:50 plasma dilution.

(G–I) As (A)–(C) but for antibody-dependent complement deposition (ADCD) assay, measuring deposited C3. A serial dilution of plasma was used, starting from 1:50 plasma dilution, with area under the curve (AUC) calculated by GraphPad Prism.

(J–L) As (A)–(C) but for antibody-dependent cellular phagocytosis (ADCP) assay, measuring THP-1 uptake of WT Spike-coated fluorescent beads incubated with plasma. A serial dilution of plasma was used, starting from 1:50 plasma dilution.

Spearman correlations (line of best fit) are drawn for all IgG1 data, and Post3 and bivalent samples for IgG4. Post2 IgG4 levels were below the limit of detection (LOD = 0.05 µg/mL), so no best-fit line is drawn. r^2 and p values calculated by GraphPad Prism. Samples paired from individuals are shown in gray. Black data points represent the geometric mean ± SD. Data representative of three technical replicates. ns, not significant; ***$p < 0.001$, ****$p < 0.0001$, paired Wilcoxon signed-rank test calculated using GraphPad Prism. See also Figures S2 and S3.

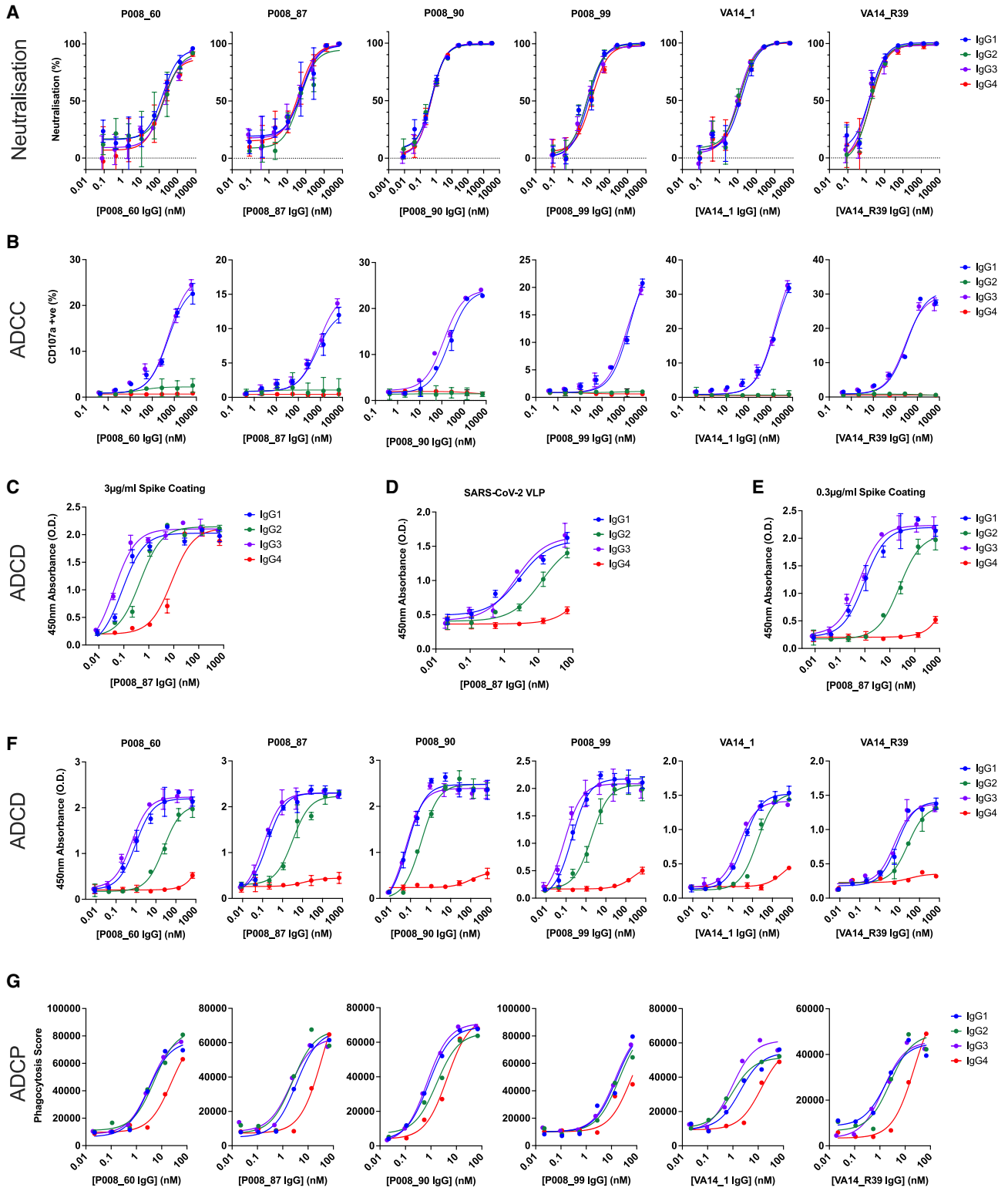

Figure 4. Functional activity of SARS-CoV-2 mAbs when expressed as different IgG subclasses

(A) Neutralization curves for mAbs P008_60, P008_87, P008_90, P008_99, VA14_1, and VA14_R39 class-switched to IgG1 (blue), IgG2 (green), IgG3 (purple), and IgG4 (red), against WT SARS-CoV-2 Spike pseudotyped virus.

(B) As (A) but for ADCC measured as percentage of NK cells with surface-accessible CD107a.

(legend continued on next page)

Neutralization of virus by IgG is largely antibody Fc-binding independent,[47] and indeed, class switching each of these SARS-CoV-2 mAbs to IgG1, IgG2, IgG3, and IgG4 had no impact on their ability to neutralize ancestral SARS-CoV-2 pseudovirus infection of HeLa-ACE2 cells (Figure 4A). Having demonstrated unchanged binding and neutralization activity, we next measured effector-function activities of the class-switched antibodies. For all six mAbs, the IgG1 and IgG3 subclasses were able to stimulate CD16 expressing NK-92 cells to degranulate in the ADCC assay as measured by CD107a cell-surface expression[48] (Figure 4B). However, IgG2 and IgG4 subclasses were not able to activate degranulation of these cells, consistent with their inability to bind to the CD16 expressing NK-92 cell line (Figure S5A).

In the complement activation assay, IgG1 and IgG3 versions of P008_87 were equally able to fix complement C3, and IgG2 and IgG4 displayed an 8-fold and 100-fold reduced complement fixation activity, respectively, when Spike was coated at 3 μg/mL (Figure 4C). When the complement deposition assay was repeated with concentrated virus-like particles (VLPs) expressing SARS-CoV-2 Spike coated on the ELISA plate, no ADCD activity of IgG4 could be detected (Figure 4D), presumably due to a lower avidity of C3q binding. This hypothesis was confirmed, as ADCD activity of the IgG4 mAbs was also absent when the recombinant Spike was coated at a lower density of 0.3 μg/mL (Figure 4E). A similar trend was observed for the remaining IgG4 mAbs on both concentrated VLPs (Figure S7) and recombinant Spike coated at 0.3 μg/mL (Figure 4F).

Finally, in the ADCP assay, equal phagocytic activity was observed for the IgG1, IgG2, and IgG3 subclasses of each mAb, but there was a 5- to 15-fold reduction in the phagocytic activity of IgG4, which is consistent with the reduced binding to the THP-1 cells (Figure 4G). Overall, the IgG4 subclass mAbs were unable to facilitate ADCC and had reduced ADCD and ADCP activity.

Non-competing IgG4 is functionally silent, not inhibitory

Antibodies function *in vivo* within a polyclonal mix of antigen-specific antibodies of different isotypes and subclasses. To determine the functional impact of Spike-specific IgG4 on overall antibody effector function of plasma, we next investigated how the mAbs of different IgG subclasses, either targeting the same epitope or non-competing epitopes, would interact with one another in effector-function assays.

First, we investigated the effect of the presence of IgG4 targeting the same epitope as an IgG1 with potent ADCC activity. We maintained a constant level of the IgG1 version of the mAb (either P008_87 or VA14_R39) prior to titrating in either additional IgG1 or IgG4 of the same mAb. Adding in additional IgG1 of the mAb led to an increased NK cell degranulation once the concentration was greater than the baseline level of mAb (Figure 5A). However, addition of the IgG4 version of the mAb binding to the same epitope led to inhibition of degranulation, likely due to competition for binding to a shared epitope on Spike. The same trend was observed for both P008_87 and VA14_R39. However, this inhibition of ADCC activity was not observed when an IgG4 targeting a non-competing epitope was added (Figure 5B). Again, a constant level of IgG1 antibody was maintained, but either an additional IgG1 or IgG4 of a non-competing mAb was added. Addition of IgG1 similarly led to additional NK cell degranulation. However, addition of IgG4 as a non-competing antibody had no effect on overall degranulation.

A similar experimental approach was used to study the direct impact of Spike-specific IgG4 on ADCD and ADCP by a potent IgG1 mAb. When IgG1 was added to a constant level of IgG1 targeting the same epitope (either P008_87 or VA14_R39), an increase in ADCD was observed. When the IgG4 version of this mAb was added there was a decrease in ADCD, indicating an inhibitory effect (Figure 5C). However, addition of an IgG1 or IgG4 targeting a different Spike epitope showed no decrease in ADCD activity (Figure 5D). In contrast, as the IgG4 version of the mAbs could facilitate ADCP, addition of competing or non-competing IgG1 or IgG4 led to an increase in ADCP (Figures 5E and 5F). Overall, the presence of Spike-specific IgG4 could potentially decrease effector-function activity (both ADCC and ADCD) through preventing the binding of IgG subclasses that are potent activators of effector functions, including IgG1.

To determine whether such an effect might be seen *in vivo* in the context of a polyclonal antibody response, we added a cocktail of the IgG4 mAbs targeting different Spike epitopes (P008_60, P008_87, P008_90, P008_99, VA14_1, and VA14_R39) to plasma collected after two mRNA doses, when the Spike-specific IgG4 level is very low (Figure S8A), or after three doses (Figures 5G–5I), and measured the impact on ADCD, ADCC, and ADCP. Pooled IgG4 or IgG1 mAbs were added at a combined concentration of 1 mg/mL, which greatly exceeds the maximum level of Spike-specific IgG4 measured in plasma. HIV-1 broadly neutralizing antibody PGT128 was also used as a negative control.[57] Addition of pooled Spike-specific IgG1 mAbs was able to increase the level of ADCC (Figures 5G and S8A) and ADCD (Figure 5H). However, although the pooled IgG4 was able to compete with the activity of IgG1 mAb P008_99, no difference in ADCC (Figures 5G and S8A) and ADCD (Figure 5H) activity was observed for the polyclonal plasma. Similar to the increase in ADCP observed in the mAb competition experiments, addition of either the IgG1 or IgG4 cocktails increased the level of ADCP (Figure 5I).

This difference in ADCC and ADCD competition between the mAbs and polyclonal plasma may be due to the recombinant

(C) ADCD assay for P008_87 as IgG1 (blue), IgG2 (green), IgG3 (purple), or IgG4 (red) with 3 μg/mL WT Spike ELISA plate coating.
(D) ADCD assay for P008_87 as IgG1 (blue), IgG2 (green), IgG3 (purple), or IgG4 (red) against Spike virus-like particles (VLP) (filled circles) or naked VLPs (clear circles).
(E) ADCD assay for P008_87 as IgG1 (blue), IgG2 (green), IgG3 (purple), or IgG4 (red) with 0.3 μg/mL WT Spike plate coating.
(F) ADCD for P008_60, P008_87, P008_90, P008_99, VA14_1, and VA14_R39 class-switched to IgG1 (blue), IgG2 (green), IgG3 (purple), and IgG4 (red) with 0.3 μg/mL WT Spike plate coating.
(G) As (A) but for ADCP, measuring THP-1 macrophage uptake of WT Spike-coated fluorescent beads incubated with antibody.
Data representative of three technical replicates, presented as geometric mean ± SD. Error bars not shown if smaller than data points. See also Figures S4–S7.

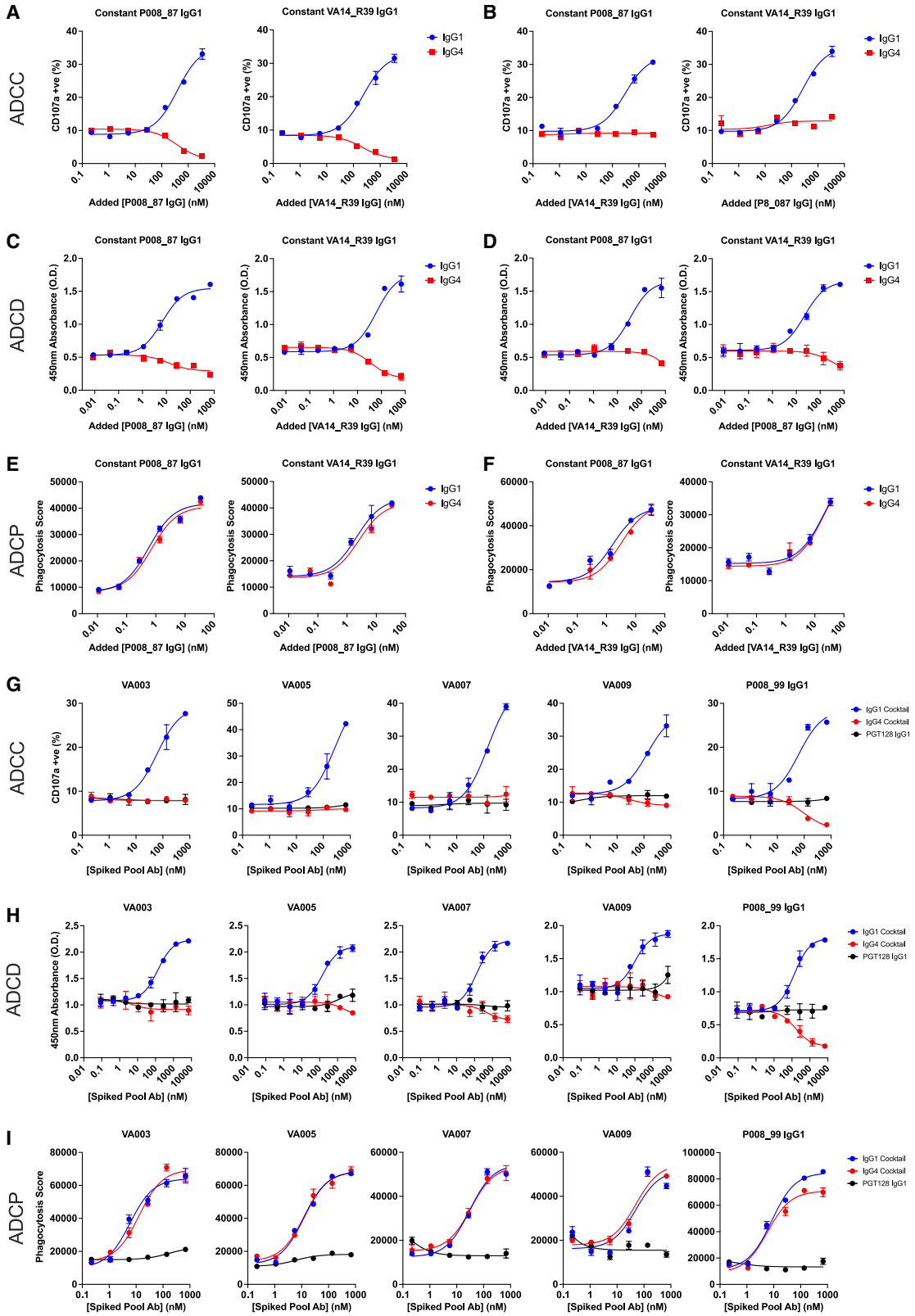

(legend on next page)

IgG4s only targeting a proportion of the potential Spike epitopes targeted by the functional IgG1 and IgG3 in the polyclonal plasma. To reduce the number of competing epitopes, the ADCC competition assay was repeated with immobilized RBD and a cocktail of four RBD-specific mAbs (P008_87, P008_90, VA14_1, and VA14_R39). While addition of the IgG1 mAb cocktail increased ADCC activity, there was a trend toward a slight decrease in plasma ADCC when the IgG4 mAb cocktail was added (Figure S8B). To determine whether the IgG4 mAb cocktail can outcompete plasma IgG1 for binding to Spike or RBD, we also performed a parallel ELISA that demonstrated an increase in overall IgG1 and IgG4 Spike or RBD binding when the IgG1 and IgG4 mAb cocktails were added to Post3 plasma but a corresponding decrease in IgG4 or IgG1 binding, respectively (Figures S9A and S9B).

These data suggest that the interplay between IgG1 and IgG4 within the context of the polyclonal sera, where there is a wider array of neutralizing and non-neutralizing epitopes targeted on Spike, is more complex.

DISCUSSION

This study supports previous observations that the COVID-19 mRNA-based vaccine, BNT162b2, can lead to a Spike-specific IgG4 response following multiple exposures.[13,23–25] This study extends these observations further through additional understanding of the factors impacting the switch to IgG4 following BNT162b2 vaccination and the functional activity and potential consequences of high levels of Spike-specific IgG4.

Comparing the kinetics and magnitude of Spike-specific IgG4 production in individuals with varying vaccination histories enabled us to identify additional factors that impact IgG4 class switching in the context of mRNA vaccination. The interval between first and second BNT162b2 dose proved important for the switch to Spike-specific IgG4, as demonstrated by an elevated level of IgG4 in the extended (12-week interval) vs. short (3-week interval) group at 6 months post second vaccine dose. However, a third BNT162b2 dose resulted in boosting to reach similar levels of Spike-specific IgG4 in both the short and extended groups. These data suggest that vaccine interval alone is not sufficient to explain the previously reported difference in production of Spike-specific IgG4 between BNT162b2 administered at a 3-week interval and AZD1222 administered at a 12-week interval, where no Spike-specific IgG4 was detected, but the difference must also be related to the vaccine type and formulation.[58] We observed the level of Spike-specific IgG4 to further increase following additional mRNA vaccination, similar to Gelderloos et al. who showed that the IgG4 level can continue to increase after up to five doses of mRNA vaccine in older adults.[24] Spike antigen exposure through BTI also increased IgG4 Spike levels. Whether these increases are due to continued evolution of already switched IgG4 or new class-switching events needs to be investigated. However, the class switch to IgG4 is specific for SARS-CoV-2 Spike in the form of an mRNA-based immunogen, as nucleoprotein-specific IgG4 was not detected following two SARS-CoV-2 BTIs, and HA-specific IgG4 was not detected in individuals co-immunized with the influenza vaccine at the time of mRNA booster vaccination. These results indicate that there may be specific conditions created by the mRNA vaccine that make B cells more prone to induce class-switch recombination (CSR) to distal subclasses. Investigation of class switching to antigen-specific IgG4 for other mRNA-based vaccines is required.

It has been proposed that long germinal-center reactions observed following mRNA vaccination, where there is a prolonged presence of the Spike antigen in the lymph node,[8,9,59] might explain the high level of Spike-specific IgG4.[25] Prolonged antigen exposure has also been proposed as the mechanism behind IgG4 responses to honeybee venom observed in beekeepers.[60] However, prolonged antigen exposure through repeated vaccination with tetanus vaccines is not sufficient to generate a strong vaccine-specific IgG4 response in the majority of individuals.[25,61,62] Furthermore, despite continued maturation of the Spike-specific IgG response being observed for at least 6 months post SARS-CoV-2 infection, presumably due to extended antigen exposure,[42] no Spike-specific IgG4 was detected in our longitudinal infection cohort, including both mild and severe disease, up to 33 weeks post infection. These observations highlight that repeated or prolonged antigen exposure is not sufficient to facilitate IgG4 switch.

The distribution in IgG4 binding to the RBD and NTD domains was similar to that observed for total IgG and IgG1, suggesting that there is no epitope bias in the subclass switching. As the IgG4 shows a similar breadth of variant

Figure 5. Effector-function competition assays between IgG1 and IgG4

(A) ADCC competition assay, with constant level of either P008_87 IgG1 or VA14_R39 IgG1 to give 10% NK cells with detectable surface CD107a, incubated with increasing amounts of the same antibody as an IgG1 (blue) or IgG4 (red).

(B) ADCC competition assay with constant level of either P008_87 IgG1 or VA14_R39 IgG1 to give 10% of NK cells with surface CD107a, incubated with increasing amounts of the other non-competitively binding antibody.

(C and D) As (A) and (B) but for ADCD.

(E and F) As (A) and (B) but for ADCP.

(G) ADCC competition assay spiking in additional pooled IgG1 or IgG4 monoclonal antibody cocktails (P008_60, P008_87, P008_90, P008_99, VA14_1, and VA14_R39) or IgG1 isotype control antibody (anti-HIV IgG1 mAb PGT128) into four volunteer plasma samples (extended group Post3 samples) at 1:100 dilution or positive control of P008_99 IgG1 monoclonal at 1 μg/mL.

(H) As (G) but for ADCD.

(I) ADCP competition assay spiking in additional pooled IgG1 or IgG4 monoclonal antibody cocktails (P008_60, P008_87, P008_90, P008_99, VA14_1, and VA14_R39) or IgG1 isotype control antibody (anti-HIV IgG1 mAb PGT128) into four volunteer plasma samples (extended group Post3 samples) at 1:2,000 dilution or positive control of P008_99 IgG1 monoclonal at 0.5 μg/mL.

Data representative of three technical replicates, plotting geometric mean ± SD. Error bars not shown if smaller than data points. See also Figures S8 and S9.

Spike binding, it also suggests that the IgG4 B cells could be arising from reactivation and switching of existing Spike-reactive B cells rather than a *de novo* response. Additionally, SARS-CoV-2 infection prior to BNT162b2 vaccination was observed to accelerate the appearance of Spike-specific IgG4, with IgG4 first being detected at low levels from 3 weeks after the first BNT162b2 dose in three of eight individuals and in all (8/8) individuals from 3 weeks after the second dose. This more rapid appearance suggests that IgG subclasses generated in response to SARS-CoV-2 infection can be class switched to IgG4 upon mRNA vaccination, indicative of reactivation of existing B cell clones rather than generation of a *de novo* response. This is similar to the late remodeling of the memory B cell repertoire observed in vaccinated individuals following BA.1 infection.[63] However, it is noteworthy that the avidity of the Spike-specific IgG4 lags behind that of the total IgG, particularly against the BA.1 variant Spike. In contrast to the former observation, this may indicate that IgG4 production does not solely arise from the class switching of high-avidity IgG subclasses and is supported by identification of variant-specific B cell clones upon BTI.[64] Alternatively, the lower avidity could also arise from the ability of IgG4 to undergo Fab arm exchange leading to monovalent antibody binding with reduced avidity.[34] Further investigations into the clonal origin of IgG4 in relation to other antibody classes and IgG subclasses over time is required to understand further the origin of IgG4.

Antibody effector functions have been shown to be important in the therapeutic and prophylactic activity of SARS-CoV-2 mAbs in animal models.[20,36] A significant concern with the elicitation of Spike-specific IgG4 is the reported anti-inflammatory properties arising from reduced affinity to Fcγ receptors[26,33] and an association with risk of SARS-CoV-2 infection.[65] Importantly, despite the production of Spike-specific IgG4, repeated mRNA vaccine boosting has remained protective from severe COVID-19.[12] The consequence of high levels of Spike-specific IgG4 on effector-function activity is difficult to tease apart, due to the polyclonal nature of plasma and the varying proportions and amounts of Spike-specific IgG1, IgG2, IgG3, and IgG4 both at different time points and between individuals as well as the lack of animal models that produce IgG4.[41] Aurelia et al. recently demonstrated that the functional impact of IgG4 is dependent upon the titer of each IgG subclass and the Fcγ receptor being studied.[66] By subclass-switching previously characterized Spike-specific IgG mAbs, we have been able to investigate the functional implications of elevated levels of Spike-specific IgG4 more directly. As expected, antibody class switching had no impact on the ability of mAbs to neutralize SARS-CoV-2, which is consistent with the increasing plasma-neutralizing activity observed as Spike-specific total IgG increases. Spike-specific IgG1 and IgG3 were able to facilitate ADCC, ADCD, and ADCP equally. Spike-specific IgG2 lost ADCC activity, retained ADCP activity, and was a weak activator of ADCD. Spike-specific IgG4 had the lowest levels of effector-function activity, showing no ADCC and ADCD activity (at low antigen densities), and had a 10-fold reduction in ADCP. Using mAbs expressed as different subclasses in ADCC and ADCD competition assays, we showed that in the context of viral infection the Spike-specific IgG4 is functionally silent unless there is direct binding competition with a functionally active IgG1. In this scenario, the IgG4 reduces effector-function activity by preventing the binding of IgG1 to the Spike antigen. In the context of allergy, increased titers of allergen-specific IgG4 has been shown to reduce hypersensitivity through blocking the activity of IgE,[67] and IgG4 in the context of mRNA vaccination may have a comparative function in reducing inflammatory responses while maintaining the ability to neutralize free virus. Indeed, this blocking nature of IgG4 makes it a commonly used format for therapeutic mAbs due to its limited ability to induce inflammatory responses.[30] Despite the unusual presence of Spike-specific IgG4, the relatively low-level presence compared to the more functionally active IgG1 suggests the inhibitory effect arising from steric occlusion could be outcompeted for the limited antigenic sites on the surface of a virion or infected cell or the lower avidity of IgG4 binding. Furthermore, in the context of SARS-CoV-2 infection, antibodies against viral proteins other than Spike can also mediate effector functions such as ADCC.[68] Therefore, the non-stimulatory effect of Spike-specific IgG4 may be hidden in more complex scenarios, such as polyclonal mixes. Indeed, we were unable to inhibit ADCD or ADCC activity in polyclonal sera through addition of a cocktail of Spike-specific IgG4s at high concentrations (up to 1 mg/mL).

In summary, we show that factors including vaccine interval and frequency, hybrid immunity, and BTI all enhance the production of Spike-specific IgG4 following BNT162b2 mRNA vaccination. Through generation of Spike-specific mAbs of each IgG subclass, we showed that IgG4 can inhibit ADCC and ADCD activity of potently activating IgG1 through direct binding competition. However, the polyclonal nature of plasma and the lower avidity of IgG4 binding observed suggest that the impact on overall effector-function activity is likely to be minimal and will be heavily dependent on the epitope specificity of the IgG4 antibodies produced. Further research is needed to understand the factors that trigger IgG4 class switching in the context of mRNA vaccination and the origin of the antigen-specific IgG4 antibodies.

Limitations of the study

Limitations of this study include the relatively small group sizes for the different vaccine and infection cohorts. This study would be strengthened through the study of IgG subclass responses to alternative COVID-19 vaccine platforms including viral vectors, inactivated virus, and subunit vaccines. The IgG1 and IgG4 mAb cocktails used in the ADCC and ADCP competition studies are unlikely to cover the full range of functional epitopes present on SARS-CoV-2 Spike, and therefore the full extent of IgG4 competition in the context of the polyclonal response may not have been reached.

RESOURCE AVAILABILITY

Lead contact

Further information and requests for resources and reagents should be directed to and will be fulfilled by the lead contact, Katie J. Doores (katie.doores@kcl.ac.uk).

Materials availability

Reagents generated in this study are available from the lead contact with a completed materials transfer agreement.

Data and code availability

Any additional information required to reanalyze the data reported in this paper is available from the lead contact upon request. This paper does not report original code.

ACKNOWLEDGMENTS

We thank Wendy Barclay for providing the Beta, Delta, and BA.1 Spike expression plasmids and James Voss for providing the HeLa-ACE2 cells. We thank Kareena Kumar for technical assistance. This work was funded by MRC project grant MR/X009041/1 to K.J.D.; MRC Genotype-to-Phenotype UK National Virology Consortium (MR/W005611/1 and MR/Y004205/1) to K.J.D.; and Wellcome funded consortium Genotype-to-Phenotype Global 226141/Z/22/Z to K.J.D. Fondation Dormeur, Vaduz funded equipment for K.J.D. K.J.D. was supported by the Medical Research Foundation Emerging Leaders Prize 2021. R.J.S. was supported by the MRC (MR/S00971X/1) and Wellcome Trust (226615/Z/22/Z).

AUTHOR CONTRIBUTIONS

Conceptualization, K.J.D. and J.C.H.T.; methodology, J.C.H.T., A.C.S., J.S., C.G., and A.K.; resources. R.J.S. and B.M.; supervision, K.J.D.; writing – original draft, K.J.D. and J.C.H.T. All authors reviewed and edited the manuscript.

DECLARATION OF INTERESTS

The authors declare no competing interests.

STAR★METHODS

Detailed methods are provided in the online version of this paper and include the following:

- KEY RESOURCES TABLE
- EXPERIMENTAL MODEL AND STUDY PARTICIPANT DETAILS
  - Ethics
  - Bacterial strains and cell culture
- METHOD DETAILS
  - Protein expression and purification
  - IgG subclass cloning and expression
  - Pseudovirus production
  - VLP production and quantification
  - Antibody subclass ELISA
  - Avidity assay
  - Immune complex binding assay
  - Neutralization assay
  - Antibody Dependent Cellular Cytotoxicity (ADCC) assay
  - Antibody Dependent Complement Deposition (ADCD) assay
  - Antibody Dependent Cellular Phagocytosis (ADCP) assay
  - IgG subclass ADCC, ADCD and ADCP competition assays
  - Plasma Spiked IgG4 ADCC, ADCD and ADCP assays
  - IgG1 and IgG4 competition ELISAs
- QUANTIFICATION AND STATISTICAL ANALYSIS

SUPPLEMENTAL INFORMATION

Supplemental information can be found online at https://doi.org/10.1016/j.celrep.2025.116000.

Received: February 17, 2025
Revised: April 30, 2025
Accepted: June 20, 2025

REFERENCES

1. Bok, K., Sitar, S., Graham, B.S., and Mascola, J.R. (2021). Accelerated COVID-19 vaccine development: milestones, lessons, and prospects. Immunity *54*, 1636–1651. https://doi.org/10.1016/j.immuni.2021.07.017.
2. Higdon, M.M., Wahl, B., Jones, C.B., Rosen, J.G., Truelove, S.A., Baidya, A., Nande, A.A., ShamaeiZadeh, P.A., Walter, K.K., Feikin, D.R., et al. (2022). A Systematic Review of Coronavirus Disease 2019 Vaccine Efficacy and Effectiveness Against Severe Acute Respiratory Syndrome Coronavirus 2 Infection and Disease. Open Forum Infect. Dis. *9*, ofac138. https://doi.org/10.1093/ofid/ofac138.
3. Polack, F.P., Thomas, S.J., Kitchin, N., Absalon, J., Gurtman, A., Lockhart, S., Perez, J.L., Pérez Marc, G., Moreira, E.D., Zerbini, C., et al. (2020). Safety and Efficacy of the BNT162b2 mRNA Covid-19 Vaccine. N. Engl. J. Med. *383*, 2603–2615. https://doi.org/10.1056/NEJMoa2034577.
4. Baden, L.R., El Sahly, H.M., Essink, B., Kotloff, K., Frey, S., Novak, R., Diemert, D., Spector, S.A., Rouphael, N., Creech, C.B., et al. (2021). Efficacy and Safety of the mRNA-1273 SARS-CoV-2 Vaccine. N. Engl. J. Med. *384*, 403–416. https://doi.org/10.1056/NEJMoa2035389.
5. UKHSA (2022). SARS-CoV-2 variants of concern and variants under investigation in England, number 34. https://assets.publishing.service.gov.uk/government/uploads/system/uploads/attachment_data/file/1050236/technical-briefing-34-14-january-2022.pdf.
6. Seow, J., Graham, C., Merrick, B., Acors, S., Pickering, S., Steel, K.J.A., Hemmings, O., O'Byrne, A., Kouphou, N., Galao, R.P., et al. (2020). Longitudinal observation and decline of neutralizing antibody responses in the three months following SARS-CoV-2 infection in humans. Nat. Microbiol. *5*, 1598–1607. https://doi.org/10.1038/s41564-020-00813-8.
7. Graham, C., Lechmere, T., Rehman, A., Seow, J., Kurshan, A., Huettner, I., Maguire, T.J.A., Tam, J.C.H., Cox, D., Ward, C., et al. (2022). The effect of Omicron breakthrough infection and extended BNT162b2 booster dosing on neutralization breadth against SARS-CoV-2 variants of concern. PLoS Pathog. *18*, e1010882. https://doi.org/10.1371/journal.ppat.1010882.
8. Kim, W., Zhou, J.Q., Horvath, S.C., Schmitz, A.J., Sturtz, A.J., Lei, T., Liu, Z., Kalaidina, E., Thapa, M., Alsoussi, W.B., et al. (2022). Germinal centre-driven maturation of B cell response to mRNA vaccination. Nature *604*, 141–145. https://doi.org/10.1038/s41586-022-04527-1.
9. Roltgen, K., Nielsen, S.C.A., Silva, O., Younes, S.F., Zaslavsky, M., Costales, C., Yang, F., Wirz, O.F., Solis, D., Hoh, R.A., et al. (2022). Immune imprinting, breadth of variant recognition, and germinal center response in human SARS-CoV-2 infection and vaccination. Cell *185*, 1025–1040. e14. https://doi.org/10.1016/j.cell.2022.01.018.
10. Sokal, A., Chappert, P., Barba-Spaeth, G., Roeser, A., Fourati, S., Azzaoui, I., Vandenberghe, A., Fernandez, I., Meola, A., Bouvier-Alias, M., et al. (2021). Maturation and persistence of the anti-SARS-CoV-2 memory B cell response. Cell *184*, 1201–1213.e14. https://doi.org/10.1016/j.cell.2021.01.050.
11. Kirsebom, F.C.M., Andrews, N., Stowe, J., Ramsay, M., and Lopez Bernal, J. (2023). Duration of protection of ancestral-strain monovalent vaccines and effectiveness of bivalent BA.1 boosters against COVID-19 hospitalisation in England: a test-negative case-control study. Lancet Infect. Dis. *23*, 1235–1243. https://doi.org/10.1016/S1473-3099(23)00365-1.
12. Lee, I.T., Cosgrove, C.A., Moore, P., Bethune, C., Nally, R., Bula, M., Kalra, P.A., Clark, R., Dargan, P.I., Boffito, M., et al. (2023). Omicron BA.1-containing mRNA-1273 boosters compared with the original COVID-19 vaccine in the UK: a randomised, observer-blind, active-controlled trial. Lancet Infect. Dis. *23*, 1007–1019. https://doi.org/10.1016/S1473-3099(23)00295-5.
13. Akhtar, M., Islam, M.R., Khaton, F., Soltana, U.H., Jafrin, S.A., Rahman, S.I.A., Tauheed, I., Ahmed, T., Khan, I.I., Akter, A., et al. (2023). Appearance of tolerance-induction and non-inflammatory SARS-CoV-2 spike-specific IgG4 antibodies after COVID-19 booster vaccinations. Front. Immunol. *14*, 1309997. https://doi.org/10.3389/fimmu.2023.1309997.

14. Parhiz, H., Atochina-Vasserman, E.N., and Weissman, D. (2024). mRNA-based therapeutics: looking beyond COVID-19 vaccines. Lancet *403*, 1192–1204. https://doi.org/10.1016/S0140-6736(23)02444-3.

15. Goldblatt, D., Alter, G., Crotty, S., and Plotkin, S.A. (2022). Correlates of protection against SARS-CoV-2 infection and COVID-19 disease. Immunol. Rev. *310*, 6–26. https://doi.org/10.1111/imr.13091.

16. Chan, C.E.Z., Seah, S.G.K., Chye, D.H., Massey, S., Torres, M., Lim, A.P. C., Wong, S.K.K., Neo, J.J.Y., Wong, P.S., Lim, J.H., et al. (2021). The Fc-mediated effector functions of a potent SARS-CoV-2 neutralizing antibody, SC31, isolated from an early convalescent COVID-19 patient, are essential for the optimal therapeutic efficacy of the antibody. PLoS One *16*, e0253487. https://doi.org/10.1371/journal.pone.0253487.

17. Pierre, C.N., Adams, L.E., Higgins, J.S., Anasti, K., Goodman, D., Mielke, D., Stanfield-Oakley, S., Powers, J.M., Li, D., Rountree, W., et al. (2024). Non-neutralizing SARS-CoV-2 N-terminal domain antibodies protect mice against severe disease using Fc-mediated effector functions. PLoS Pathog. *20*, e1011569. https://doi.org/10.1371/journal.ppat.1011569.

18. Schafer, A., Muecksch, F., Lorenzi, J.C.C., Leist, S.R., Cipolla, M., Bournazos, S., Schmidt, F., Maison, R.M., Gazumyan, A., Martinez, D.R., et al. (2021). Antibody potency, effector function, and combinations in protection and therapy for SARS-CoV-2 infection in vivo. J. Exp. Med. *218*, e20201993. https://doi.org/10.1084/jem.20201993.

19. Yamin, R., Jones, A.T., Hoffmann, H.H., Schäfer, A., Kao, K.S., Francis, R. L., Sheahan, T.P., Baric, R.S., Rice, C.M., Ravetch, J.V., and Bournazos, S. (2021). Fc-engineered antibody therapeutics with improved anti-SARS-CoV-2 efficacy. Nature *599*, 465–470. https://doi.org/10.1038/s41586-021-04017-w.

20. Gorman, M.J., Patel, N., Guebre-Xabier, M., Zhu, A.L., Atyeo, C., Pullen, K. M., Loos, C., Goez-Gazi, Y., Carrion, R., Jr., Tian, J.H., et al. (2021). Fab and Fc contribute to maximal protection against SARS-CoV-2 following NVX-CoV2373 subunit vaccine with Matrix-M vaccination. Cell Rep. Med. *2*, 100405. https://doi.org/10.1016/j.xcrm.2021.100405.

21. Tostanoski, L.H., Wegmann, F., Martinot, A.J., Loos, C., McMahan, K., Mercado, N.B., Yu, J., Chan, C.N., Bondoc, S., Starke, C.E., et al. (2020). Ad26 vaccine protects against SARS-CoV-2 severe clinical disease in hamsters. Nat. Med. *26*, 1694–1700. https://doi.org/10.1038/s41591-020-1070-6.

22. Mercado, N.B., Zahn, R., Wegmann, F., Loos, C., Chandrashekar, A., Yu, J., Liu, J., Peter, L., McMahan, K., Tostanoski, L.H., et al. (2020). Single-shot Ad26 vaccine protects against SARS-CoV-2 in rhesus macaques. Nature *586*, 583–588. https://doi.org/10.1038/s41586-020-2607-z.

23. Buhre, J.S., Pongracz, T., Künsting, I., Lixenfeld, A.S., Wang, W., Nouta, J., Lehrian, S., Schmelter, F., Lunding, H.B., Dühring, L., et al. (2022). mRNA vaccines against SARS-CoV-2 induce comparably low long-term IgG Fc galactosylation and sialylation levels but increasing long-term IgG4 responses compared to an adenovirus-based vaccine. Front. Immunol. *13*, 1020844. https://doi.org/10.3389/fimmu.2022.1020844.

24. Gelderloos, A.T., Verheul, M.K., Middelhof, I., de Zeeuw-Brouwer, M.L., van Binnendijk, R.S., Buisman, A.M., and van Kasteren, P.B. (2024). Repeated COVID-19 mRNA vaccination results in IgG4 class switching and decreased NK cell activation by S1-specific antibodies in older adults. Immun. Ageing *21*, 63. https://doi.org/10.1186/s12979-024-00466-9.

25. Irrgang, P., Gerling, J., Kocher, K., Lapuente, D., Steininger, P., Habenicht, K., Wytopil, M., Beileke, S., Schäfer, S., Zhong, J., et al. (2023). Class switch toward noninflammatory, spike-specific IgG4 antibodies after repeated SARS-CoV-2 mRNA vaccination. Sci. Immunol. *8*, eade2798. https://doi.org/10.1126/sciimmunol.ade2798.

26. Pillai, S. (2023). Is it bad, is it good, or is IgG4 just misunderstood? Sci. Immunol. *8*, eadg7327. https://doi.org/10.1126/sciimmunol.adg7327.

27. Urban, M., Winkler, T., Landini, M.P., Britt, W., and Mach, M. (1994). Epitope-specific distribution of IgG subclasses against antigenic domains on glycoproteins of human cytomegalovirus. J. Infect. Dis. *169*, 83–90. https://doi.org/10.1093/infdis/169.1.83.

28. Qin, L., Tang, L.F., Cheng, L., and Wang, H.Y. (2022). The clinical significance of allergen-specific IgG4 in allergic diseases. Front. Immunol. *13*, 1032909. https://doi.org/10.3389/fimmu.2022.1032909.

29. Motta, R.V., and Culver, E.L. (2024). IgG4 autoantibodies and autoantigens in the context of IgG4-autoimmune disease and IgG4-related disease. Front. Immunol. *15*, 1272084. https://doi.org/10.3389/fimmu.2024.1272084.

30. Rispens, T., and Huijbers, M.G. (2023). The unique properties of IgG4 and its roles in health and disease. Nat. Rev. Immunol. *23*, 763–778. https://doi.org/10.1038/s41577-023-00871-z.

31. van de Veen, W., Globinska, A., Jansen, K., Straumann, A., Kubo, T., Verschoor, D., Wirz, O.F., Castro-Giner, F., Tan, G., Rückert, B., et al. (2020). A novel proangiogenic B cell subset is increased in cancer and chronic inflammation. Sci. Adv. *6*, eaaz3559. https://doi.org/10.1126/sciadv.aaz3559.

32. Bruhns, P., Iannascoli, B., England, P., Mancardi, D.A., Fernandez, N., Jorieux, S., and Daëron, M. (2009). Specificity and affinity of human Fcgamma receptors and their polymorphic variants for human IgG subclasses. Blood *113*, 3716–3725. https://doi.org/10.1182/blood-2008-09-179754.

33. Vidarsson, G., Dekkers, G., and Rispens, T. (2014). IgG subclasses and allotypes: from structure to effector functions. Front. Immunol. *5*, 520. https://doi.org/10.3389/fimmu.2014.00520.

34. van der Neut Kolfschoten, M., Schuurman, J., Losen, M., Bleeker, W.K., Martínez-Martínez, P., Vermeulen, E., den Bleker, T.H., Wiegman, L., Vink, T., Aarden, L.A., et al. (2007). Anti-inflammatory activity of human IgG4 antibodies by dynamic Fab arm exchange. Science *317*, 1554–1557. https://doi.org/10.1126/science.1144603.

35. Beaudoin-Bussieres, G., and Finzi, A. (2024). Deciphering Fc-effector functions against SARS-CoV-2. Trends Microbiol. *32*, 756–768. https://doi.org/10.1016/j.tim.2024.01.005.

36. Zhang, A., Stacey, H.D., D'Agostino, M.R., Tugg, Y., Marzok, A., and Miller, M.S. (2023). Beyond neutralization: Fc-dependent antibody effector functions in SARS-CoV-2 infection. Nat. Rev. Immunol. *23*, 381–396. https://doi.org/10.1038/s41577-022-00813-1.

37. Winkler, E.S., Gilchuk, P., Yu, J., Bailey, A.L., Chen, R.E., Chong, Z., Zost, S.J., Jang, H., Huang, Y., Allen, J.D., et al. (2021). Human neutralizing antibodies against SARS-CoV-2 require intact Fc effector functions for optimal therapeutic protection. Cell *184*, 1804–1820.e16. https://doi.org/10.1016/j.cell.2021.02.026.

38. Clark, J.J., Hoxie, I., Adelsberg, D.C., Sapse, I.A., Andreata-Santos, R., Yong, J.S., Amanat, F., Tcheou, J., Raskin, A., Singh, G., et al. (2024). Protective effect and molecular mechanisms of human non-neutralizing cross-reactive spike antibodies elicited by SARS-CoV-2 mRNA vaccination. Cell Rep. *43*, 114922. https://doi.org/10.1016/j.celrep.2024.114922.

39. DiLillo, D.J., Tan, G.S., Palese, P., and Ravetch, J.V. (2014). Broadly neutralizing hemagglutinin stalk-specific antibodies require FcgammaR interactions for protection against influenza virus in vivo. Nat. Med. *20*, 143–151. https://doi.org/10.1038/nm.3443.

40. Van den Hoecke, S., Ehrhardt, K., Kolpe, A., El Bakkouri, K., Deng, L., Grootaert, H., Schoonooghe, S., Smet, A., Bentahir, M., Roose, K., et al. (2017). Hierarchical and Redundant Roles of Activating FcgammaRs in Protection against Influenza Disease by M2e-Specific IgG1 and IgG2a Antibodies. J. Virol. *91*, e02500-16. https://doi.org/10.1128/JVI.02500-16.

41. Olivieri, D.N., and Gambón Deza, F. (2018). Immunoglobulin genes in Primates. Mol. Immunol. *101*, 353–363. https://doi.org/10.1016/j.molimm.2018.07.020.

42. Gaebler, C., Wang, Z., Lorenzi, J.C.C., Muecksch, F., Finkin, S., Tokuyama, M., Cho, A., Jankovic, M., Schaefer-Babajew, D., Oliveira, T.Y., et al. (2021). Evolution of antibody immunity to SARS-CoV-2. Nature *591*, 639–644. https://doi.org/10.1038/s41586-021-03207-w.

43. Walls, A.C., Park, Y.J., Tortorici, M.A., Wall, A., McGuire, A.T., and Veesler, D. (2020). Structure, Function, and Antigenicity of the SARS-CoV-2 Spike Glycoprotein. Cell *183*, 1735. https://doi.org/10.1016/j.cell.2020.11.032.

44. Jackson, C.B., Farzan, M., Chen, B., and Choe, H. (2022). Mechanisms of SARS-CoV-2 entry into cells. Nat. Rev. Mol. Cell Biol. *23*, 3–20. https://doi.org/10.1038/s41580-021-00418-x.

45. Wratil, P.R., Stern, M., Priller, A., Willmann, A., Almanzar, G., Vogel, E., Feuerherd, M., Cheng, C.C., Yazici, S., Christa, C., et al. (2022). Three exposures to the spike protein of SARS-CoV-2 by either infection or vaccination elicit superior neutralizing immunity to all variants of concern. Nat. Med. *28*, 496–503. https://doi.org/10.1038/s41591-022-01715-4.

46. Muecksch, F., Wang, Z., Cho, A., Gaebler, C., Ben Tanfous, T., DaSilva, J., Bednarski, E., Ramos, V., Zong, S., Johnson, B., et al. (2022). Increased Memory B Cell Potency and Breadth After a SARS-CoV-2 mRNA Boost. Nature *607*, 128–134. https://doi.org/10.1038/s41586-022-04778-y.

47. Mozdzanowska, K., Feng, J., and Gerhard, W. (2003). Virus-neutralizing activity mediated by the Fab fragment of a hemagglutinin-specific antibody is sufficient for the resolution of influenza virus infection in SCID mice. J. Virol. *77*, 8322–8328. https://doi.org/10.1128/jvi.77.15.8322-8328.2003.

48. Bartsch, Y.C., Cizmeci, D., Kang, J., Gao, H., Shi, W., Chandrashekar, A., Collier, A.R.Y., Chen, B., Barouch, D.H., and Alter, G. (2023). Selective SARS-CoV2 BA.2 escape of antibody Fc/Fc-receptor interactions. iScience *26*, 106582. https://doi.org/10.1016/j.isci.2023.106582.

49. Alter, G., Malenfant, J.M., and Altfeld, M. (2004). CD107a as a functional marker for the identification of natural killer cell activity. J. Immunol. Methods *294*, 15–22. https://doi.org/10.1016/j.jim.2004.08.008.

50. Polycarpou, A., Wagner-Gamble, T., Greenlaw, R., O' Neill, L.A., Khan, H., Malim, M., Romano, M., Smolarek, D., Doores, K., Wallis, R., et al. (2023). The complement pattern recognition molecule CL-11 promotes invasion and injury of respiratory epithelial cells by SARS-CoV-2. Preprint at bioRxiv. https://doi.org/10.1101/2023.12.11.571109.

51. Zohar, T., Atyeo, C., Wolf, C.R., Logue, J.K., Shuey, K., Franko, N., Choi, R. Y., Wald, A., Koelle, D.M., Chu, H.Y., et al. (2022). A multifaceted high-throughput assay for probing antigen-specific antibody-mediated primary monocyte phagocytosis and downstream functions. J. Immunol. Methods *510*, 113328. https://doi.org/10.1016/j.jim.2022.113328.

52. Graham, C., Seow, J., Huettner, I., Khan, H., Kouphou, N., Acors, S., Winstone, H., Pickering, S., Galao, R.P., Dupont, L., et al. (2021). Neutralization potency of monoclonal antibodies recognizing dominant and subdominant epitopes on SARS-CoV-2 Spike is impacted by the B.1.1.7 variant. Immunity *54*, 1276–1289.e6. https://doi.org/10.1016/j.immuni.2021.03.023.

53. Seow, J., Graham, C., Hallett, S.R., Lechmere, T., Maguire, T.J.A., Huettner, I., Cox, D., Khan, H., Pickering, S., Roberts, R., et al. (2022). ChAdOx1 nCoV-19 vaccine elicits monoclonal antibodies with cross-neutralizing activity against SARS-CoV-2 viral variants. Cell Rep. *39*, 110757. https://doi.org/10.1016/j.celrep.2022.110757.

54. Barnes, C.O., Jette, C.A., Abernathy, M.E., Dam, K.M.A., Esswein, S.R., Gristick, H.B., Malyutin, A.G., Sharaf, N.G., Huey-Tubman, K.E., Lee, Y. E., et al. (2020). SARS-CoV-2 neutralizing antibody structures inform therapeutic strategies. Nature *588*, 682–687. https://doi.org/10.1038/s41586-020-2852-1.

55. Cassel, D.L., Keller, M.A., Surrey, S., Schwartz, E., Schreiber, A.D., Rappaport, E.F., and McKenzie, S.E. (1993). Differential expression of Fc gamma RIIA, Fc gamma RIIB and Fc gamma RIIC in hematopoietic cells: analysis of transcripts. Mol. Immunol. *30*, 451–460. https://doi.org/10.1016/0161-5890(93)90113-.

56. Fleit, H.B., and Kobasiuk, C.D. (1991). The human monocyte-like cell line THP-1 expresses Fc gamma RI and Fc gamma RII. J. Leukoc. Biol. *49*, 556–565. https://doi.org/10.1002/jlb.49.6.556.

57. Walker, L.M., Huber, M., Doores, K.J., Falkowska, E., Pejchal, R., Julien, J. P., Wang, S.K., Ramos, A., Chan-Hui, P.Y., Moyle, M., et al. (2011). Broad neutralization coverage of HIV by multiple highly potent antibodies. Nature *477*, 466–470. https://doi.org/10.1038/nature10373.

58. Hartley, G.E., Fryer, H.A., Gill, P.A., Boo, I., Bornheimer, S.J., Hogarth, P. M., Drummer, H.E., O'Hehir, R.E., Edwards, E.S.J., and van Zelm, M.C. (2024). Homologous but not heterologous COVID-19 vaccine booster elicits IgG4+ B-cells and enhanced Omicron subvariant binding. NPJ Vaccines *9*, 129. https://doi.org/10.1038/s41541-024-00919-8.

59. Turner, J.S., O'Halloran, J.A., Kalaidina, E., Kim, W., Schmitz, A.J., Zhou, J.Q., Lei, T., Thapa, M., Chen, R.E., Case, J.B., et al. (2021). SARS-CoV-2 mRNA vaccines induce persistent human germinal centre responses. Nature *596*, 109–113. https://doi.org/10.1038/s41586-021-03738-2.

60. Aalberse, R.C., van der Gaag, R., and van Leeuwen, J. (1983). Serologic aspects of IgG4 antibodies. I. Prolonged immunization results in an IgG4-restricted response. J. Immunol. *130*, 722–726.

61. Unger, P.P., Makuch, M., Aalbers, M., Derksen, N.I.L., Ten Brinke, A., Aalberse, R.C., Rispens, T., and van Ham, S.M. (2018). Repeated vaccination with tetanus toxoid of plasma donors with pre-existing specific IgE transiently elevates tetanus-specific IgE but does not induce allergic symptoms. Clin. Exp. Allergy *48*, 479–482. https://doi.org/10.1111/cea.13107.

62. Devey, M.E., Bleasdale, K.M., French, M.A., and Harrison, G. (1985). The IgG4 subclass is associated with a low affinity antibody response to tetanus toxoid in man. Immunology *55*, 565–567.

63. Sokal, A., Barba-Spaeth, G., Hunault, L., Fernández, I., Broketa, M., Meola, A., Fourati, S., Azzaoui, I., Vandenberghe, A., Lagouge-Roussey, P., et al. (2023). SARS-CoV-2 Omicron BA.1 breakthrough infection drives late remodeling of the memory B cell repertoire in vaccinated individuals. Immunity *56*, 2137–2151.e7. https://doi.org/10.1016/j.immuni.2023.07.007.

64. Alsoussi, W.B., Malladi, S.K., Zhou, J.Q., Liu, Z., Ying, B., Kim, W., Schmitz, A.J., Lei, T., Horvath, S.C., Sturtz, A.J., et al. (2023). SARS-CoV-2 Omicron boosting induces de novo B cell response in humans. Nature *617*, 592–598. https://doi.org/10.1038/s41586-023-06025-4.

65. Martin Perez, C., Ruiz-Rius, S., Ramirez-Morros, A., Vidal, M., Opi, D.H., Santamaria, P., Blanco, J., Vidal-Alaball, J., Beeson, J.G., Molinos-Albert, L.M., et al. (2025). Post-vaccination IgG4 and IgG2 class switch associates with increased risk of SARS-CoV-2 infections. J. Infect. *90*, 106473. https://doi.org/10.1016/j.jinf.2025.106473.

66. Aurelia, L.C., Purcell, R.A., Theisen, R.M., Kelly, A., Esterbauer, R., Ramanathan, P., Lee, W.S., Wines, B.D., Hogarth, P.M., Juno, J.A., et al. (2025). Increased SARS-CoV-2 IgG4 has variable consequences dependent upon Fc function, Fc receptor polymorphism, and viral variant. Sci. Adv. *11*, eads1482. https://doi.org/10.1126/sciadv.ads1482.

67. Santos, A.F., James, L.K., Bahnson, H.T., Shamji, M.H., Couto-Francisco, N.C., Islam, S., Houghton, S., Clark, A.T., Stephens, A., Turcanu, V., et al. (2015). IgG4 inhibits peanut-induced basophil and mast cell activation in peanut-tolerant children sensitized to peanut major allergens. J. Allergy Clin. Immunol. *135*, 1249–1256. https://doi.org/10.1016/j.jaci.2015.01.012.

68. Fielding, C.A., Sabberwal, P., Williamson, J.C., Greenwood, E.J.D., Crozier, T.W.M., Zelek, W., Seow, J., Graham, C., Huettner, I., Edgeworth, J.D., et al. (2022). SARS-CoV-2 host-shutoff impacts innate NK cell functions, but antibody-dependent NK activity is strongly activated through non-spike antibodies. eLife *11*, e74489. https://doi.org/10.7554/eLife.74489.

69. Rosa, A., Pye, V.E., Graham, C., Muir, L., Seow, J., Ng, K.W., Cook, N.J., Rees-Spear, C., Parker, E., Dos Santos, M.S., et al. (2021). SARS-CoV-2 can recruit a haem metabolite to evade antibody immunity. Sci. Adv. *7*, eabg7607. https://doi.org/10.1126/sciadv.abg7607.

70. Rogers, T.F., Zhao, F., Huang, D., Beutler, N., Burns, A., He, W.T., Limbo, O., Smith, C., Song, G., Woehl, J., et al. (2020). Isolation of potent SARS-CoV-2 neutralizing antibodies and protection from disease in a small animal model. Science *369*, 956–963. https://doi.org/10.1126/science.abc7520.

71. Tiller, T., Meffre, E., Yurasov, S., Tsuiji, M., Nussenzweig, M.C., and Wardemann, H. (2008). Efficient generation of monoclonal antibodies from single human B cells by single cell RT-PCR and expression vector cloning. J. Immunol. Methods *329*, 112–124. https://doi.org/10.1016/j.jim.2007.09.017.

72. Scheid, J.F., Mouquet, H., Feldhahn, N., Seaman, M.S., Velinzon, K., Pietzsch, J., Ott, R.G., Anthony, R.M., Zebroski, H., Hurley, A., et al. (2009). Broad diversity of neutralizing antibodies isolated from memory B cells in HIV-infected individuals. Nature *458*, 636–640. https://doi.org/10.1038/nature07930.

73. von Boehmer, L., Liu, C., Ackerman, S., Gitlin, A.D., Wang, Q., Gazumyan, A., and Nussenzweig, M.C. (2016). Sequencing and cloning of antigen-specific antibodies from mouse memory B cells. Nat. Protoc. *11*, 1908–1923. https://doi.org/10.1038/nprot.2016.102.

74. Brouwer, P.J.M., Caniels, T.G., van der Straten, K., Snitselaar, J.L., Aldon, Y., Bangaru, S., Torres, J.L., Okba, N.M.A., Claireaux, M., Kerster, G., et al. (2020). Potent neutralizing antibodies from COVID-19 patients define multiple targets of vulnerability. Science *369*, 643–650. https://doi.org/10.1126/science.abc5902.

75. Demaison, C., Parsley, K., Brouns, G., Scherr, M., Battmer, K., Kinnon, C., Grez, M., and Thrasher, A.J. (2002). High-level transduction and gene expression in hematopoietic repopulating cells using a human immunodeficiency [correction of imunodeficiency] virus type 1-based lentiviral vector containing an internal spleen focus forming virus promoter. Hum. Gene Ther. *13*, 803–813. https://doi.org/10.1089/10430340252898984.

76. Zufferey, R., Nagy, D., Mandel, R.J., Naldini, L., and Trono, D. (1997). Multiply attenuated lentiviral vector achieves efficient gene delivery in vivo. Nat. Biotechnol. *15*, 871–875. https://doi.org/10.1038/nbt0997-871.

77. Aricescu, A.R., Lu, W., and Jones, E.Y. (2006). A time- and cost-efficient system for high-level protein production in mammalian cells. Acta Crystallogr. D Biol. Crystallogr. *62*, 1243–1250. https://doi.org/10.1107/S0907444906029799.

78. Howarth, M., Liu, W., Puthenveetil, S., Zheng, Y., Marshall, L.F., Schmidt, M.M., Wittrup, K.D., Bawendi, M.G., and Ting, A.Y. (2008). Monovalent, reduced-size quantum dots for imaging receptors on living cells. Nat. Methods *5*, 397–399. https://doi.org/10.1038/nmeth.1206.

79. Wilson, C., Ebling, R., Henig, C., Adler, T., Nicolaevski, R., Barak, M., Cazabon, J., Maisin, D., Lepoutre, T., Gruson, D., et al. (2013). Significant, quantifiable differences exist between IgG subclass standards WHO67/97 and ERM-DA470k and can result in different interpretation of results. Clin. Biochem. *46*, 1751–1755. https://doi.org/10.1016/j.clinbiochem.2013.07.014.

80. Zelek, W.M., Harris, C.L., and Morgan, B.P. (2018). Extracting the barbs from complement assays: Identification and optimisation of a safe substitute for traditional buffers. Immunobiology *223*, 744–749. https://doi.org/10.1016/j.imbio.2018.07.016.

STAR★METHODS

KEY RESOURCES TABLE

REAGENT or RESOURCE	SOURCE	IDENTIFIER
Antibodies		
Goat-anti-human-Fc-AP	Jackson	RRID: AB_2337608 Cat#:109-055-098
F(ab')$_2$ Fragment Goat Anti-Human IgG, F (ab')$_2$ fragment specific	Jackson	RRID: AB_2337545 Cat#: 109-106-106
Mouse-anti-human-IgG1-HRP	Thermo Fisher Scientific	RRID: AB_2534051 Cat#: A-10648
Mouse-anti-human-IgG2-HRP	Thermo Fisher Scientific	RRID: AB_10376169 Cat#: MH1722
Mouse-anti-human-IgG3-HRP	SouthernBiotech	RRID: AB_2796699 Cat#: 9210-05
Mouse-anti-human-IgG4-HRP	Thermo Fisher Scientific	RRID: AB_2539714 Cat#: MH1742
Fc Block (Clone Fc1)	BD Biosciences	RRID:AB_2728082 Cat# 564219
PerCP/Cyanine5.5 anti-human CD107a antibody (Clone H4A3)	Biolegend	RRID:AB_2296838 Cat#: 328616
Goat-anti-Guinea Pig Complement C3 polyclonal	MP Bio	RRID:AB_2334449 Cat#: 0855371
Mouse-anti-Goat-IgG-HRP	Santa Cruz Biotechnology	RRID:AB_628490 Cat#: sc-2354
mAbs P008_60, P008_87, P008_90, P008_99, VA14_1 and VA14_R39	This manuscript and ref. [52,53]	N/A
Bacterial and virus strains		
NEB® Stable Competent *E. coli*	New England Biolabs	Cat#: C3040H
Biological samples		
ERM-DA470k Serum Antibody Standard	Sigma	Cat#: ERMDA470KIFCC
Vaccinee plasma and convalescent serum	This manuscript	N/A
Chemicals, peptides, and recombinant proteins		
Polyethylenimine, Linear, MW 25000 (PEI Max)	Polysciences, Inc	Cat#: 23966
Polyethylenimine Hydrochloride, Linear, MW 4,000	Polysciences, Inc	Cat#: 24885
Recombinant Stabilized SARS-CoV-2 Spike for ELISA (Wuhan, BA1)	This manuscript and ref. [53]	N/A
Recombinant SARS-CoV-2 Spike Receptor Binding Domain (RBD) for ELISA (Wuhan)	Refs.[6,69]	N/A
Recombinant SARS-CoV-2 Spike N-terminal Domain (NTD) (residues 1-310) for ELISA (Wuhan)	Refs.[6,69]	N/A
Recombinant SARS-CoV-2 Nucleocapsid (N protein) for ELISA (Wuhan)	Gift from Dr Leo James (MRC LMB, Cambridge)	N/A
Recombinant SARS-CoV-2 Spike (biotinylated)	Refs.[52,53]	N/A
Recombinant Influenza HA hemagluttinin A/California 04/2009 for ELISA	This manuscript	N/A
Protein G agarose	GE Healthcare	Cat#: Cytiva 17-0618-02
HiTrap IMAC columns	GE Healthcare	Cat#: Cytiva 17-0921-04

(*Continued on next page*)

Continued

REAGENT or RESOURCE	SOURCE	IDENTIFIER
HILOAD 16/600 SUPERDEX 200 PG Column	GE Healthcare	Cat#: 28989335
Strep-TactinXT Superflow 50% Suspension	IBA Lifesciences	Cat#: 2-4010-002
BioLock blocking solution	IBA Lifesciences	Cat#: 2-0205-050
Ni Sepharose 6 Fast Flow	Cytiva	Cat#: GE17-5318-06
Golgistop Protein Transport Inhibitor	BD Biosciences	Cat#: 554724
Critical commercial assays		
Q5® Site-Directed Mutagenesis Kit	New England Biolabs	Cat#: E0554
Bright-Glo luciferase kit	Promega	Cat#: E2610
Phusion High-Fidelity DNA Polymerase	New England Biolabs	Cat#: E2611L
LIVE/DEAD Fixable Aqua Dead Cell Stain Kit	Thermofisher Scientific	Cat#: L34957
1-Step™ Ultra TMB ELISA Substrate Solution	Thermofisher Scientific	Cat#: 34028
Phosphatase substrate	Sigma Aldrich	Cat#: S0942-200TAB
Guinea Pig Complement Serum	Sigma	Cat#: S1639
FluoSpheres™ NeutrAvidin™-Labeled Microspheres, 1.0 μm, yellow-green fluorescent (505/515)	Invitrogen	Cat#: F8776
Experimental models: Cell lines		
FreeStyle™ 293F Cells	Thermofisher Scientific	RRID:CVCL_D603 Cat#: R79007
HEK293T/17	ATCC	RRID:CVCL_1926 Cat#: CRL-11268
HeLa-ACE2	James Voss (Scripps) [70]	N/A
NK-92 Cells transduced with high affinity (Valine 158) human CD16	This manuscript (Source: Richard Stanton)	N/A
THP-1 Cells	ATCC	RRID:CVCL_0006 Cat#: TIB-202
Raji Cells	ATCC	RRID:CVCL_0511 Cat#: CCL-86
Oligonucleotides		
Antibody variable sequence primers	Refs. [53,71–73]	N/A
Recombinant DNA		
Biotinylated Spike (pHLSec)	This manuscript and ref. [53]	N/A
Pre-fusion, stabilized and uncleaved SARS-CoV-2 Spike (pcDNA3.1+) (WT)	Marit van Gils (Amsterdam)[74]	N/A
Truncated SARS-CoV-2 Wuhan Spike (pcDNA3.1+)	Wendy Barclay (Imperial)	N/A
Truncated B.1.1.529 (omicron/BA.1) variant Spike (pcDNA3.1+)	Wendy Barclay (Imperial)	N/A
Full-length SARS-CoV-2 Spike (pcDNA3.1+)	Ref.[6]	N/A
pHIV-Luc (constructed by replacing GFP in pHR'SIN-SEW (Demaison et al.[75]) with HA-luciferase)	Luis Apolonia (KCL)	N/A
HIV 8.91 gag/pol packaging construct	p8.91 [76]	N/A
HIV 8.91 mScarlet gag/pol packaging construct	Sergi Padilla-Parra (KCL)	N/A
AbVec2.0-IGHG2 Heavy Chain Plasmid	Addgene	RRID:Addgene_99576

(*Continued on next page*)

Continued

REAGENT or RESOURCE	SOURCE	IDENTIFIER
AbVec2.0-IGHG3 Heavy Chain Plasmid	Addgene	RRID:Addgene_99577
AbVec2.0-IGHG4 Heavy Chain Plasmid	Addgene	RRID:Addgene_99578
BirA Plasmid (pDisplay-BirA-ER)	Addgene	RRID:Addgene_20856
Software and algorithms		
FlowJo	Tree Star	https://www.flowjo.com
Prism	Graphpad	https://www.graphpad.com/scientific-software/prism/
Other		
FACS Canto II	BD Biosciences	N/A
Victor^{TM} X3 multilabel reader	Perkin Elmer	N/A

EXPERIMENTAL MODEL AND STUDY PARTICIPANT DETAILS

Ethics

Demographics of the vaccinated and infected volunteer samples are shown in Table S1. Samples were collected according to the timeline shown in Figure S1. This vaccine cohort used human plasma samples collected with written consent as part of a study entitled "Antibody responses following COVID-19 vaccination." Ethical approval was obtained from the King's College London Infectious Diseases Biobank (IDB) (KDJF-110121) under the terms of the IDB's ethics permission (REC ref. 19/SC/0232) granted by the South Central Hampshire B Research Ethics Committee in 2019 and London Bridge Research Ethics Committee (reference: REC14/LO/1699). Collection of surplus serum samples from SARS-CoV-2 convalescent donors at St Thomas Hospital, London, was approved by South Central-Hampshire B REC (20/SC/0310).

Bacterial strains and cell culture

SARS-CoV-2 pseudotypes were produced by transfection of HEK293T/17 cells (ATCC CRL-11268) and neutralization activity assayed using HeLa cells stably expressing ACE2 (kind gift from Dr James Voss, Scripps Research, CA). Monoclonal antibodies were expressed in HEK293 Freestyle (HEK293F) cells (Thermofisher Scientific). NK-92 human CD16 cells were made by transducing NK-92 cells with a retroviral vector expressing high affinity (Valine 158) human CD16. THP-1 (TIB-202) and Raji (CCL-86) cells were obtained from ATCC. HEK293T/17 cells and HeLa-ACE2 cells were maintained in Dulbecco's Modified Eagle Medium supplemented with GlutaMAX, 10% Fetal Calf Serum and 1% Penicillin/Streptomycin (DMEM-C). HEK293F cells were maintained in Freestyle media. THP-1 and Raji cells were maintained in Roswell Park Memorial Institute (RPMI) 1640 supplemented with GlutaMAX, 10% Fetal Calf Serum (RPMI-C). NK-92 cells expressing CD16 were maintained in Minimum Essential Medium α (MEM α) supplemented with L-glutamine, nucleosides, 12.5% Fetal Calf Serum, 12.5% Horse Serum, 20 mM HEPES, 0.2 mM Myo-inositol, 0.02 mM Folic Acid, 0.1 mM 2-mercaptoethanol and 50 IU/mL interleukin (IL)-2. Bacterial transformations for class switching were performed with NEB Stable Competent *E. coli*.

METHOD DETAILS

Protein expression and purification

Recombinant Spike, RBD and NTD (residues 1-310) were expressed and purified as previously described.[6,69] Recombinant SARS-CoV-2 WT Nucleocapsid (N protein) was a kind gift from Dr Leo James, Laboratory of Molecular Biology, Cambridge. Recombinant Spike trimers were engineered from full-length Spike expression plasmids (pcDNA3.1 plasmid) using a molecular cloning approach. The furin cleavage site (RRAR) was replaced with a flexible linker (GGGG), and the K986 and V987 residues in the S2 subunit were mutated to prolines using site-directed mutagenesis. The resulting sequences were truncated at amino acid position 1138 and subcloned into pHLSec[77] via Gibson assembly, positioning them upstream of a flexible linker (GSGG), T4 foldon trimerization domain, and incorporating Avi and His tags.

Biotinylated Spike was expressed as previously described.[52] Biotinylated Spike was expressed in 1L of HEK293F cells (Invitrogen) at a density of 1.5×10^6 cells/mL. To achieve *in vivo* biotinylation, 480μg of each plasmid was co-transfected with 120 μg of BirA[78] and 12 mg PEI-Max (1 mg/mL solution, Polysciences) in the presence of 200 μM biotin (final concentration). The supernatant was harvested after 7 days and purified using immobilized metal affinity chromatography and size-exclusion chromatography. Complete biotinylation was confirmed via depletion of protein using avidin beads.

Influenza HA hemagluttinin A/California 04/2009 was cloned into the pHLSec vector containing a 6xHIS tag, and expressed and purified in the same manner as for SARS-CoV-2 Spike.

IgG subclass cloning and expression

SARS-CoV-2 monoclonal antibodies were isolated and characterized previously.[7,52,53] Heavy chains were PCR amplified using previously described primers and conditions,[7,52,53,71] and cloned into human IgG heavy chains of IgG2 (Addgene AbVec2.0-IGHG2 #99576), IgG3 (AbVec2.0-IGHG3 #99577) and IgG4 (AbVec2.0-IGHG4 #99578) using the Gibson Assembly Master Mix (NEB) following the manufacturer's protocol. AbVec2.0-IGHG2, AbVec2.0-IGHG3 and AbVec2.0-IGHG4 were a gift from Hedda Wardemann (Addgene plasmid #99576, #99577 and #99578; RRID:Addgene_99576, RRID:Addgene_99577 and RRID:Addgene_99578).

Ab heavy and light plasmids were co-transfected at a 1:1 ratio into HEK-293F cells (Thermofisher) using PEI Max (1 mg/mL, Polysciences, Inc.) at a 3:1 ratio (PEI Max:DNA). Ab supernatants were harvested five days following transfection, filtered and purified using protein G affinity chromatography following the manufacturer's protocol (GE Healthcare).

Pseudovirus production

HEK293T/17 cells were seeded in a 10cm dish at a density of 3×10^5 cells/mL. Following overnight culture, cells were co-transfected using 90 μg PEI-Max (1 mg/mL, Polysciences) with 15 μg HIV-luciferase plasmid, 10 μg HIV 8.91 gag/pol plasmid, and 5 μg SARS-CoV-2 Spike protein plasmid.[76] Transfected cells were incubated for 72 h at 37°C, and virus was harvested, sterile filtered, and stored at −80°C until required.

VLP production and quantification

HEK293T/17 cells were seeded in a 10 cm dish at a density of 3×10^5 cells/mL. Cells were transfected using 90μL PEI (1mg/mL solution) with the following plasmids: 2.5 μg WT SARS-CoV-2 Spike plasmid, 8 μg HIV gag/pol mScarlet plasmid, 2 μg HIV 8.91 gag/pol plasmid, and 10 μg HIV-luciferase plasmid. The supernatant containing the VLPs was collected 72 h post-transfection, clarified by centrifugation at 3,000×g for 15 min and passed through a 0.45 μm filter. The clarified supernatant was then layered onto a sucrose cushion (20% sucrose, 50 mM Tris-HCl, 0.5 mM EDTA, and 100 mM NaCl in PBS, pH 7.4) and centrifuged at 10,000×g for 4 h at 4°C. The supernatant was gently aspirated and the concentrated VLPs were resuspended in PBS. The samples were then stored at −80°C until use. Infectivity of VLPs was measured using HeLa ACE2 cells.

Antibody subclass ELISA

High-binding ELISA plates (Corning, 3690) were coated with antigen (N protein, S glycoprotein, RBD, NTD or Influenza HA) or $F(ab')_2$ Fragment of Goat Anti-Human IgG $F(ab')_2$ fragment (Jackson 109-106-106) at 3 μg/mL (25 μL per well) in phosphate-buffered serum (PBS) overnight at 4°C. Wells were washed with PBS-T (PBS with 0.05% Tween-20) and then blocked with 100 μL of 5% milk in PBS-T for 1 h at room temperature. The wells were emptied, and serial dilutions of plasma (starting at 1:25 dilution, 5-fold dilution series, heat-inactivated at 56°C for 30 min) were added and incubated for 1 h at room temperature. Dilutions of a known monoclonal antibody standard, and serum antibody standard ERM-DA470k (Sigma)[79] were used for quantification. Wells were washed with PBS-T. Secondary antibodies were added (1:1,000 dilution in 5% Milk in PBS-T) and incubated for 1 h at room temperature, including goat-anti-human total IgG-alkaline phosphatase (AP) (Jackson Immunoresearch, 109-055-098), mouse-anti-human IgG1-horseradish peroxidase (HRP) (Invitrogen A10648), mouse-anti-human IgG2-HRP (Invitrogen MH1722), mouse-anti-human IgG3-HRP (Southern Biotech 9210-05), mouse-anti-human IgG4-HRP (Invitrogen MH174225)). Wells were washed with PBS-T and either AP substrate (Sigma) was added and read at 405 nm (AP) or one-step 3,3′,5,5′-tetramethylbenzidine (TMB) substrate (Thermo Fisher Scientific) was added and quenched with 0.5 M H_2SO_4 before reading at 450 nm (HRP). Quantification was conducted by comparing dilutions to reach the same EC_{50} value calculated by GraphPad Prism.

Avidity assay

The avidity ELISA was carried out as described above except for one additional step. After incubation of plasma, one half of the plate was incubated with 8M Urea and the other half incubated with PBS for 15 min before washing 5-times with PBS-T. The area under the curve was determined in Prism (Log dilution). The avidity index was calculated using the following formula:

$$Avidity\ index\ =\ 100 * \left(\frac{Area\ under\ curve\ with\ 8M\ Urea}{Area\ under\ curve\ with\ no\ Urea} \right)$$

Immune complex binding assay

NK-92 cells expressing human CD16, THP-1 cells and Raji cells were plated at 1.0×10^5cells/well on high-binding full-well 96 well plates. Immune complexes were formed by incubating 25 μL of serially diluted mAb in RPMI-C (starting at 100 μg/mL, 5-fold dilution series), with WT Spike protein (25 μL at 3.0 μg/mL) for 1 h. Immune complexes were then incubated with each cell type for 1 h. Cells were then washed with PBS-T, and blocked with Fc Block (BD Biosciences) for 1 h. Following a final was in PBS-T, binding to cells was measured using the same secondary antibodies as for ELISA above.

Neutralization assay

Serial dilutions of plasma samples (starting at 1:50 dilution, 5-fold dilution series, heat inactivated at 56°C for 30 min) or monoclonal antibody were prepared in DMEM-C (to total 25 μL) and incubated with pseudotyped virus (25 μL) for 1 h at 37°C in half-area 96-well

plates. HeLa ACE2 cells were diluted to a concentration of 5×10^5cells/mL and added to each well (25 μL/well), and plates incubated at 37°C for 72h. Infection levels were quantified by lysing the cells and measuring luciferase activity using the Bright-Glo Luciferase Assay Kit (Promega) on a Victor X3 multilabel plate reader (PerkinElmer).

Antibody Dependent Cellular Cytotoxicity (ADCC) assay

ADCC assay was adapted from Bartsch et al.[48] and Alter et al.[49] High-binding full-well ELISA plates were coated with Spike or RBD protein at 3 μg/mL (50 μL per well) in PBS for 2h at 37°C. Wells were washed with PBS and then blocked with 100 μL of 5% bovine serum albumin in PBS overnight at 4°C. The plates were then washed with PBS, prior to addition of serial dilutions of heat inactivated plasma samples (starting at 1:50 dilution, 5-fold dilution series) or monoclonal antibody diluted in DMEM-C and incubated at room temperature for 1 h. NK-92 CD16 cells were added (1.0×10^5 cells/well) in media supplemented with an increased IL-2 concentration (100 IU/mL), Golgistop protein transport inhibitor (BD Biosciences #554724, 5 μL per 1.0×10^6cells) and PerCP/Cyanine5.5 anti-human CD107a antibody (Biolegend Clone H4A3). Golgistop was added to maximize CD107a signal, by blocking degradation of reinternalized CD107a from the plasma membrane.[49] Plates were incubated at 37°C, 5% CO_2 for 6 h. NK-92 cells were transferred to 75 mm Polystyrene Tubes, washed with PBS and fixed by addition of 4% paraformaldehyde. Level of CD107a surface expression was measured by flow cytometry using a BD Canto II.

Antibody Dependent Complement Deposition (ADCD) assay

ADCD assay was adapted from Polycarpou et al.[50] High-binding ELISA plates (Corning, 3690) were coated with Spike protein at 3 μg/mL or 0.3 μg/mL (25 μL per well) in phosphate-buffered saline (PBS) overnight at 4°C. For VLP assays, purified VLPs at 4×10^6 infectious units/well were incubated at room temperature for 2 h. Wells were washed with PBS-T (PBS with 0.05% Tween 20) and then blocked with 100 μL of 5% milk in PBS-T for 1 h at room temperature. Serial dilutions of heat-inactivated plasma (starting at 1:250 dilution, 5-fold dilution series) or mAbs (25 μL in PBS) were added and incubated for 1 h at room temperature, followed by washing with PBS-T. Guinea Pig Complement Serum (Sigma S1639) was diluted to 1:100 (as per the complement activity level) in HEPES Buffered Saline (0.01 M HEPES, 0.15 M NaCl, 135 nM $CaCl_2$, 1 mM $MgCl_2$, adjusted to pH 7.4) as barbitone buffers are not available.[80] Diluted complement was added to the wells, alongside a heat inactivated control plasma (56°C for 30 min), and plate was incubated for 1 h. Wells were washed with PBS-T, prior to addition of Goat Anti-Guinea Pig Complement C3 polyclonal (1:250 in 5% milk/PBS-T, MP Biomedicals 0855371) for 1 h at room temperature. Wells were washed with PBS-T, and incubated with HRP-conjugated Mouse Anti-Goat IgG (1:500, Santa Cruz Biotechnology sc-2354). Wells were then washed and TMB substrate added which was quenched with 0.5 M H_2SO_4 before reading at 450 nm (HRP).

Antibody Dependent Cellular Phagocytosis (ADCP) assay

The ADCP assay was based on previously published protocol.[51] Briefly, biotinylated SARS-CoV-2 Spike (5 μL at 1 mg/mL) was incubated with 10 μL of washed yellow-green fluorescent NeutrAvidin-Labeled Microspheres (480-505 nm, 1.0 μm size, Thermofisher), and incubated at 37°C for 2 h. Beads were washed twice (0.1% PBS-BSA) by centrifugation (16,000×g, 5 min) at room temperature. The antigen-coupled fluorescent beads were resuspended in 0.1% PBS-BSA (1:500 by volume). 2.5 μL of this bead suspension was incubated with 5 μL heat inactivated diluted plasma (starting at 1:2,500 dilution, 5-fold dilution series) or antibody dilutions at room temperature for 1 h. THP-1 cells (25,000 cells/well) and bead/plasma mixes were added to 24 well plates and incubated for 16 h at 37°C, 5% CO_2. Cells were washed and non-internalized fluorescence was quenched with the addition of 0.5% trypan blue. Bead uptake was measured by flow cytometry using a BD FACS Canto II. Phagocytosis scores were determined by first plotting the antibody concentration or plasma dilution against the geometric mean fluorescence intensity of the bead positive THP-1 cells multiplied by the percent of bead positive THP-1 cells. These curves were used to calculate the AUC using GraphPad Prism.

IgG subclass ADCC, ADCD and ADCP competition assays

For competition assays, IgG1 of P008_87 or VA14_R39 were titrated to either 10% NK-92 cell degranulation activity, 25% complement C3 detection (0.5 at 450 nm absorbance) or 10% THP-1 cells with 1 or more beads for ADCP. Further P008_87 or VA14_R39 of IgG1 or IgG4 subclass was then added into this antibody mixture at different serial dilutions. These antibody mixes were then used in the ADCC and ADCD assays as described above.

Plasma Spiked IgG4 ADCC, ADCD and ADCP assays

P008_60, P008_87, P008_90, P008_99, VA14_1 and VA14_R39 IgG1s or IgG4s were pooled together for a combined final concentrations of 1 mg/mL for the anti-Spike ADCC and ADCD assays. P008_87, P008_90, VA14_1 and VA14_R39 IgG1s or IgG4s were pooled together at a final concentration of 1 mg/mL each for the RBD ADCC assays. An IgG1 isotype control of PGT128 (an anti-HIV-1 mAb) was also used to spike into plasma. The IgG1 and IgG4 cocktails were serially diluted (ADCC dilutions started from a further dilution to 100 μg/mL (685 nM), while ADCD assays started from the initial 1 mg/mL (6,850 nM)) and 25 μL added to either Post2 or Post3 plasma samples (25 μL of ED_{25} values calculated from a prior ADCD assay (roughly 1:100 dilution)). P008_99 IgG1 mAb was used at 1 μg/mL as an ADCD and ADCC positive control. P008_87 IgG1 mAb used at 1 μg/mL (6.85 nM) was used as a positive control for the RBD only ADCC assay.

Plasma Spiked ADCP assays were carried out with pools of P008_60, P008_87, P008_90, P008_99, VA14_1 and VA14_R39 IgG1s or IgG4s at final concentrations of 1 mg/mL for each assay. These were further diluted to 100 μg/mL (685 nM), before creating a 5-fold dilution series, and added to Post3 plasma samples (25 μL of ED_{25} values calculated from a prior ADCP assay (roughly 1:2,000 dilution)). P008_99 IgG1 mAb was used at 0.1 μg/mL (0.69 nM) as a positive control for the ADCP assay. 2.5 μL of these mixes were incubated with biotinylated-Spike-coated fluorescent beads as described for the standard ADCP assay.

IgG1 and IgG4 competition ELISAs

Competition ELISAs (in parallel with competition ADCC assays) were carried out by applying the Post3 plasma samples with spiked IgG1 and IgG4 cocktails to ELISA plates coated with Full WT Spike or RBD domains at 3 μg/mL (25 μL per well). The increase or decrease in bound IgG1 and IgG4 antibody upon addition of the IgG1 or IgG4 mAb cocktail was detected using the same secondary antibodies described above.

QUANTIFICATION AND STATISTICAL ANALYSIS

All ELISA, neutralization, ADCC, ADCP and ADCD experiments were performed in duplicate or triplicate as stated in the figure legends. The 50% inhibitory concentrations/dilutions (IC/ID_{50}, EC/ED_{50}) and area under curve (AUC) were calculated using GraphPad Prism software. Linear correlations (Figures 3 and S3, Spearman correlation) were calculated using GraphPad Prism. D'Agostino and Pearson tests were performed to determine normality, and based on this result, paired t-tests, multiple comparisons repeated-measures ANOVA, and Wilcoxon signed rank tests (Figures 2 and 3) were used to determine significance, also calculated using GraphPad Prism.

Cell Reports, Volume *44*

Supplemental information

Spike-specific IgG4 generated post BNT162b2 mRNA vaccination is inhibitory when directly competing with functional IgG subclasses

Jerry C.H. Tam, Abbie C. Sibayan, Jeffrey Seow, Carl Graham, Ashwini Kurshan, Blair Merrick, Richard J. Stanton, and Katie J. Doores

Supplementary Figures for:

Spike-specific IgG4 generated post BNT162b2 mRNA vaccination is inhibitory when directly competing with functional IgG subclasses

Jerry C. H. Tam[1], Abbie C. Sibayan[1], Jeffrey Seow[1], Carl Graham[1], Ashwini Kurshan[1], Blair Merrick[2], Richard J. Stanton[3], Katie J. Doores[1#]

[1] Department of Infectious Diseases, School of Immunology & Microbial Sciences, King's College London, London, UK.
[2] Centre for Clinical Infection and Diagnostics Research, Department of Infectious Diseases, Guy's and St Thomas' NHS Foundation Trust, London, UK.
[3] Division of Infection and Immunity, School of Medicine, Cardiff University, Cardiff, United Kingdom.

[#] Corresponding author: katie.doores@kcl.ac.uk

Supplementary Table S1

A)

Group	Short Group	Extended	6 Month Waning	Prior Infection	Breakthrough Infection	Bivalent Booster
Number	8	17	9	8	9	8
Gender Male : Female	1:7	7:10	4:5	3:5	3:6	1:7
Age Range (Median)	29-57 (46)	23-66 (47)	23-66 (47)	25-58 (33)	24-58 (29)	25-66 (48)

B)

Group	Mild Infection	Severe Infection
Number	11	14
Gender Male : Female	5:6	11:3
Age Range (Median)	27-67* (41)*	25-83 (55)

Supplementary Table 1 – **(A)** Demographics of the volunteers in each of the vaccination cohort groups. **(B)** Demographics for volunteers in Mild and Severe Infection groups. *= age data only available for 5 volunteers in this group. Related to Fig. 1 and Supplementary Figure S1.

Supplementary Figure S1

A)

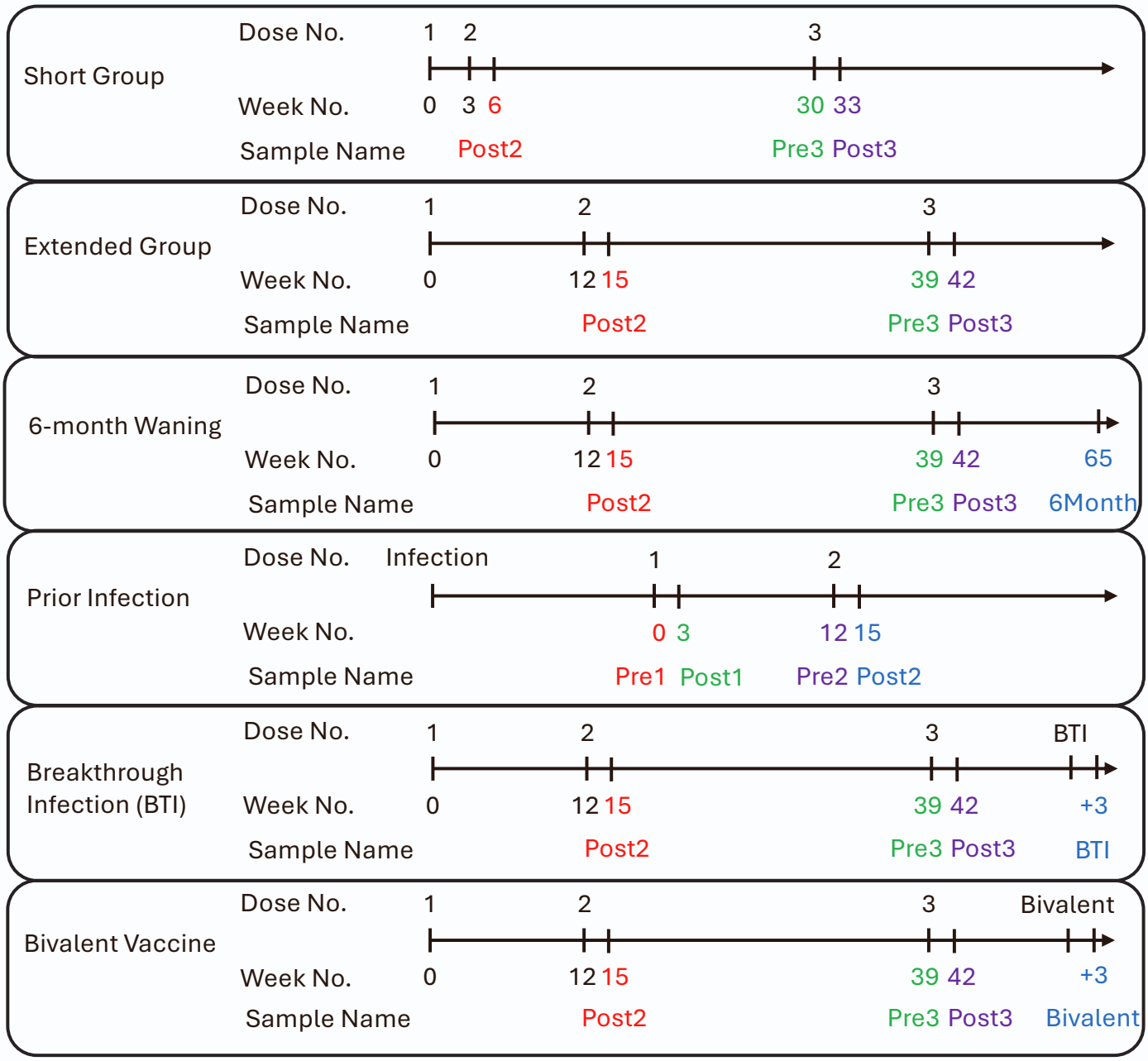

B)

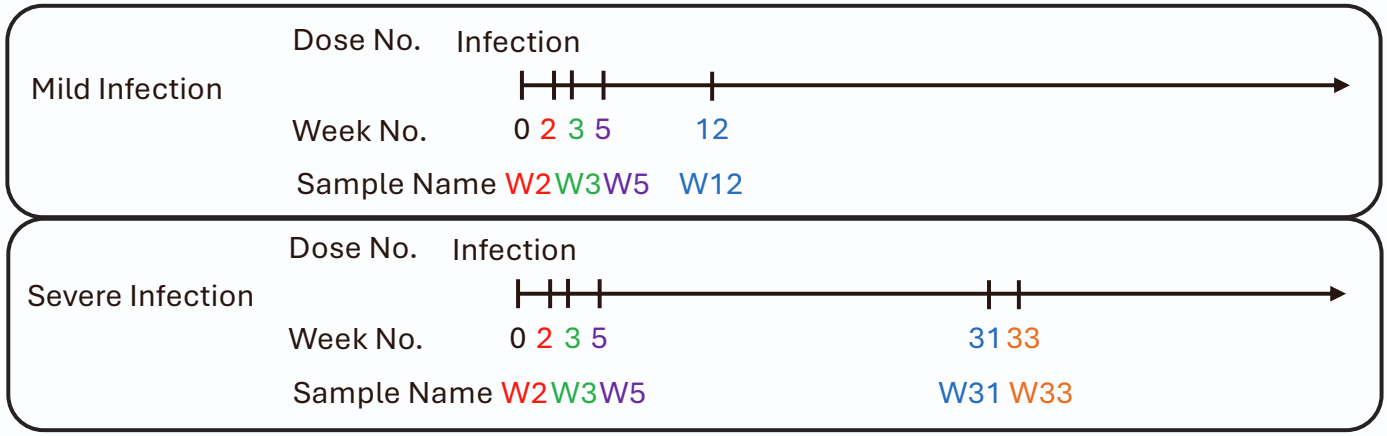

Supplementary Figure S1

Supplementary Figure S1 – **(A)** Timing of vaccinations and infection in each of our vaccinated groups. Plasma was collected in these groups at the specified times: Pre1 = before 1st dose, Post1 = 3 weeks after 1st dose, Pre2 = before 2nd dose, Post2 = 3 weeks after 2nd dose, Pre3 = before 3rd dose, Post3 = 3 weeks after 3rd dose, 6Month = 6 months after 3rd dose, BTI = 3 weeks after breakthrough infection after 3rd dose, Bivalent = 3 weeks after bivalent booster. **(B)** Timings of serum samples from mild and severe infection groups. Related to Fig.1 and Supplementary Table S1.

Supplementary Table S2

Total IgG	Post2							Pre3						
PBS-treated AUC	5.419	3.380	1.864	2.371	2.584	1.957	1.752	3.574	1.598	1.927	2.600	1.731	1.414	1.705
8M Urea-treated AUC	3.799	2.227	1.019	1.327	1.461	1.202	1.072	2.508	1.306	1.349	1.952	1.236	1.123	1.125
Avidity Index (%)	70.11	65.89	54.67	55.97	56.54	61.42	61.19	70.17	81.73	70.01	75.08	71.40	79.42	65.98
Total IgG	**Post3**							**Bivalent**						
PBS-treated AUC	3.340	1.801	2.472	3.362	2.504	2.200	2.259	4.190	2.837	4.440	3.688	3.259	3.582	3.705
8M Urea-treated AUC	2.882	1.351	2.146	2.984	2.045	1.654	1.565	3.815	2.146	3.974	3.368	2.948	3.195	3.128
Avidity Index (%)	86.29	75.01	86.81	88.76	81.67	75.18	69.28	91.05	75.64	89.50	91.32	90.46	89.20	84.43

IgG1	Post2							Pre3						
PBS-treated AUC	4.597	2.686	1.172	1.681	1.002	1.291	1.093	2.824	1.070	1.731	2.208	1.328	0.9126	1.538
8M Urea-treated AUC	3.360	1.370	0.7846	1.107	0.613	0.7437	0.6491	2.188	0.793	1.131	1.747	1.027	0.6224	0.9811
Avidity Index (%)	73.09	51.01	66.95	65.85	61.18	57.61	59.39	77.48	74.11	65.34	79.12	77.33	68.20	63.79
IgG1	**Post3**							**Bivalent**						
PBS-treated AUC	3.011	1.334	2.195	3.062	2.226	1.924	1.992	3.501	2.300	3.813	3.051	2.649	2.954	3.086
8M Urea-treated AUC	2.59	1.0533	1.869	2.376	1.771	1.279	1.384	3.097	1.825	3.326	2.734	2.325	2.252	2.312
Avidity Index (%)	86.02	78.96	85.15	77.60	79.56	66.48	69.48	88.46	79.35	87.23	89.61	87.77	76.24	74.92

IgG4	Post2							Pre3						
PBS-treated AUC	n.d.	n.d.	n.d.	n.d.	n.d.	n.d.	n.d.	2.492	0.9372	0.447	2.806	1.239	1.390	2.481
8M Urea-treated AUC	n.d.	n.d.	n.d.	n.d.	n.d.	n.d.	n.d.	0.8666	0.2899	0.1839	1.341	0.3789	0.340	0.8746
Avidity Index (%)	-	-	-	-	-	-	-	34.78	30.93	41.14	47.79	30.58	24.46	35.25
IgG4	**Post3**							**Bivalent**						
PBS-treated AUC	5.419	3.38	1.864	2.371	1.784	1.957	1.752	4.369	1.633	1.162	3.492	1.876	2.425	3.648
8M Urea-treated AUC	3.939	2.357	1.198	1.327	1.081	1.332	1.172	3.961	1.4474	0.9268	3.029	1.6401	2.058	3.170
Avidity Index (%)	72.69	69.73	64.27	55.97	60.59	68.06	66.89	90.66	88.63	79.76	86.74	87.43	84.87	86.90

Supplementary Table 2 – Avidity Area Under the Curve (AUC) calculations corresponding to Fig. 2H & Fig. 2I; for Spike-binding antibodies in Bivalent group plasma of Total IgG (black), IgG1 (blue) and IgG4 (red) subclasses, after treating with PBS or 8M Urea. 5-fold serial dilution of plasma started at 1 in 25. Only binding curves reaching saturation, with calculatable IC50 values used for this analysis, n.d. (not determined) used to denote samples not meeting this criteria. The area under the curve was determined in Prism (Log dilution). Related to Fig. 2H + 2I.

Supplementary Table S3

WT

Total IgG	Post3								Bivalent							
PBS-treated AUC	2.538	0.8199	2.138	2.358	1.971	1.818	1.775	1.716	1.929	1.241	1.548	2.029	1.161	3.876	4.190	5.660
8M Urea-treated AUC	1.827	0.6369	1.836	1.793	1.778	1.650	1.689	1.237	1.373	0.9247	1.475	1.477	1.174	3.591	3.348	5.313
Avidity Index (%)	71.99	77.68	85.89	76.02	90.18	90.76	95.18	72.10	71.18	74.51	95.28	72.79	101.12	92.65	79.90	93.87
IgG4	**Post3**								**Bivalent**							
PBS-treated AUC	2.799	1.176	1.294	6.066	3.654	1.778	3.068	1.735	5.904	1.998	1.299	5.067	2.202	3.807	6.045	1.575
8M Urea-treated AUC	2.034	0.818	0.8325	3.354	2.217	1.205	2.055	0.9573	5.249	1.542	1.148	4.134	1.944	3.293	4.662	1.322
Avidity Index (%)	72.67	69.59	64.30	55.29	60.67	67.81	66.99	55.17	88.90	77.18	88.34	81.59	88.28	86.49	77.12	83.91

BA.1

Total IgG	Post3								Bivalent							
PBS-treated AUC	2.336	1.022	2.124	2.204	1.937	1.800	1.847	1.892	1.643	1.080	1.543	1.455	1.617	2.581	2.471	4.221
8M Urea-treated AUC	1.785	0.795	1.562	2.153	1.872	1.625	1.376	1.607	1.173	0.8283	1.192	1.278	1.160	2.339	2.252	3.555
Avidity Index (%)	76.43	77.74	73.52	97.69	96.67	90.25	74.49	84.93	71.39	76.69	77.25	87.84	71.74	90.62	91.14	84.22
IgG4	**Post3**								**Bivalent**							
PBS-treated AUC	1.456	1.517	1.711	3.984	1.685	1.388	2.496	1.971	4.263	1.205	1.088	3.738	1.613	1.970	4.236	1.045
8M Urea-treated AUC	0.9522	1.038	0.9105	1.776	1.147	0.9294	1.979	1.094	3.144	0.8624	0.600	1.721	0.8807	1.424	2.630	0.6348
Avidity Index (%)	65.38	68.40	53.21	44.58	68.09	66.98	79.27	55.53	73.75	71.55	55.13	46.03	54.61	72.32	62.08	60.73

Supplementary Table 3 – Avidity Area Under the Curve (AUC) calculations corresponding to Fig. 2J; for WT and BA.1 variant Spike-binding antibodies in Bivalent group plasma of Total IgG (black), and IgG4 (red) subclass, after treating with PBS or 8M Urea. 5-fold serial dilution of plasma started at 1 in 25. Only binding curves reaching saturation, with calculatable IC50 values used for this analysis, n.d. (not determined) used to denote samples not meeting this criteria. The area under the curve was determined in Prism (Log dilution). Related to Fig. 2J.

Supplementary Figure S2

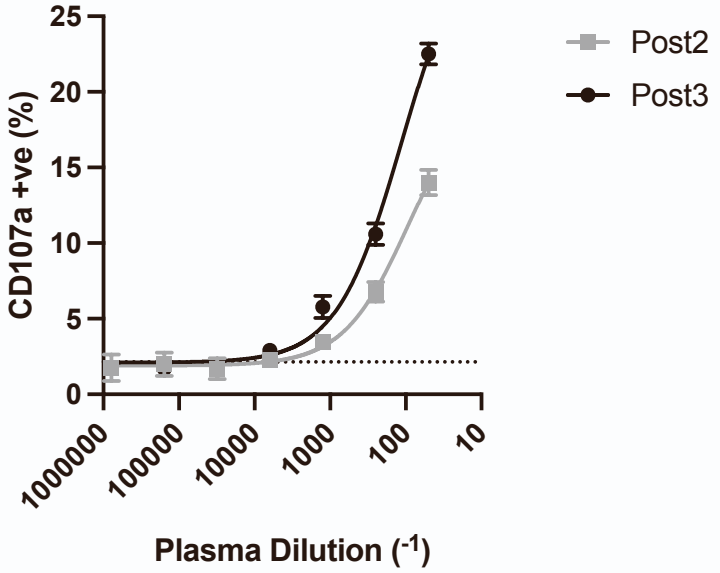

Supplementary Figure S2 – Example ADCC assay with a 5-fold serial titration of plasma from either Post2 (grey) or Post3 (black) starting at 1 in 50 dilution. Highest, non-saturating, non-Hook effect degranulation result (measured by percentage surface-expressed CD107a positive NK cells) used in correlation calculations in other figures. Data in duplicate, plotting geometric mean and standard deviation. Related to Fig. 3D and 3E.

Supplementary Figure S3

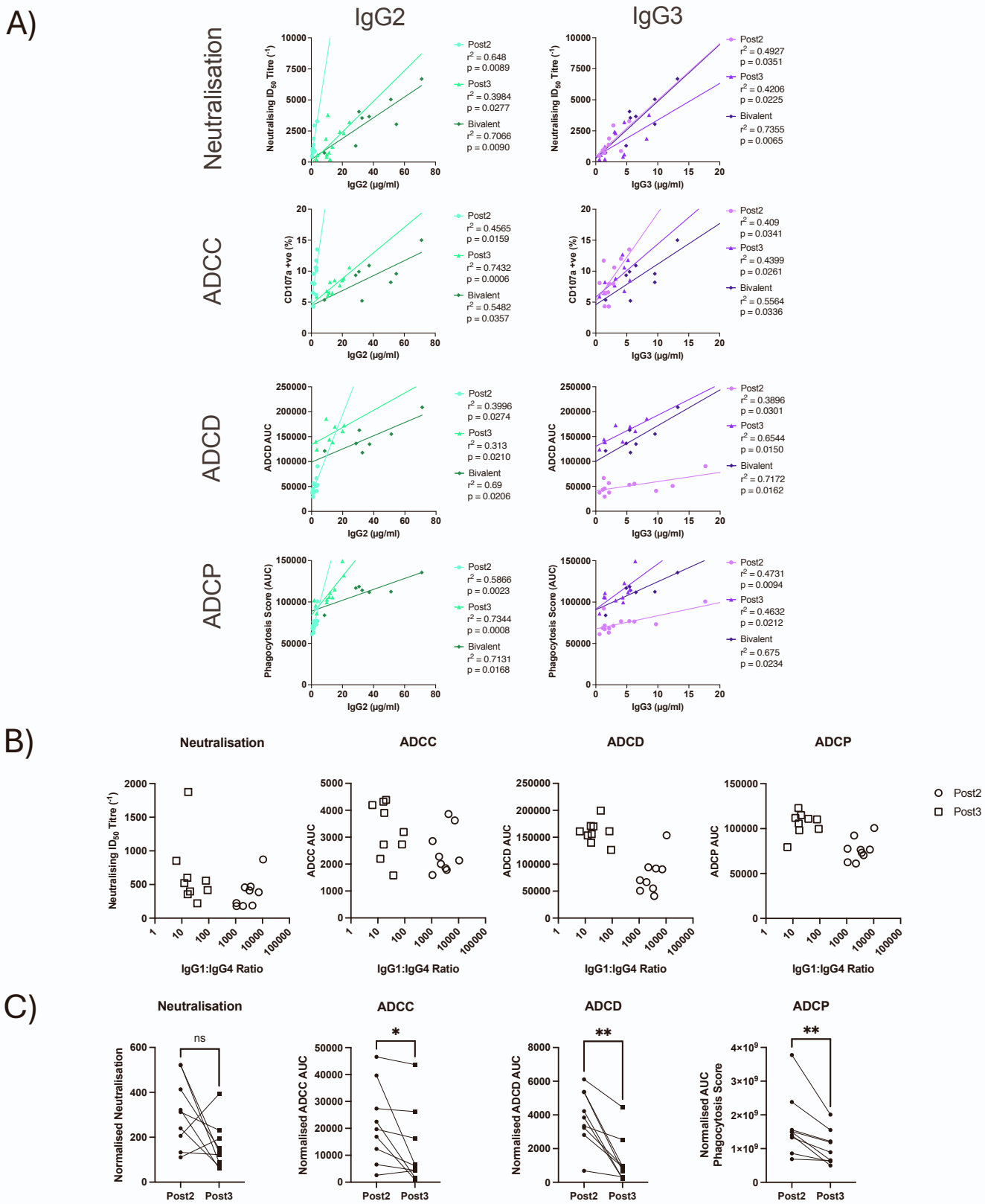

Supplementary Figure S3 – (A) Correlations between measured IgG2 and IgG3 levels and Neutralisation, ADCC, ADCD and ADCP for combined data from extended and bivalent groups. (B) Neutralisation, ADCC, ADCD, and ADCP for the extended group, plotted against the IgG1 to IgG4 ratio. Undetectable IgG4 levels were treated as the limit of detection (0.05µg/ml) to calculate values. (C) Neutralisation and ADCC normalised to 1µg/ml Spike-binding Total IgG equivalent; calculated by the activity value divided by the Total IgG level in µg/ml at Post2 or Post3 level. ADCD and ADCP calculated by conversion of dilution series to µg/ml equivalents at Post2 and Post3 level; and recalculating AUC for these new curves. ns not significant, * p<0.05, ** p<0.01. Related to Fig. 3.

Supplementary Figure S4

A)

mAb Name	VA14_1	VA14_R39	P008_90	P008_15	P008_38	P008_87	P008_96	P003_27	P008_56	P008_60	P008_2	P008_14	P008_99	P008_6
Specificity	RBD	RBD	RBD	RBD	RBD	RBD	RBD	NTD	NTD	Non-S1	NTD	NTD	NTD	Non-S1
Competition Group	1	1	3	4	4	4	4	6	6	7	ND	ND	ND	ND
Antibody Class	4	4	1 / 2	3	3	3	3	-	-	-	-	-	-	-
WT Spike ELISA EC50 (µg/ml)	0.0358	0.0585	0.0182	0.0337	0.0578	0.0212	0.0299	0.0039	0.0602	0.0311	0.0084	0.0662	0.0222	0.1
WT SARS-CoV-2 Neutralisation IC50 (µg/ml)	7.34	0.07	0.0709	0.0553	0.11	4.96	9.09	1.64	0.0136	32.9	>100	1.81	0.943	>100

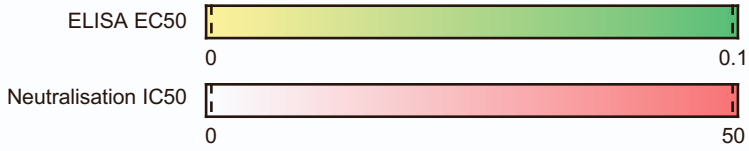

B)

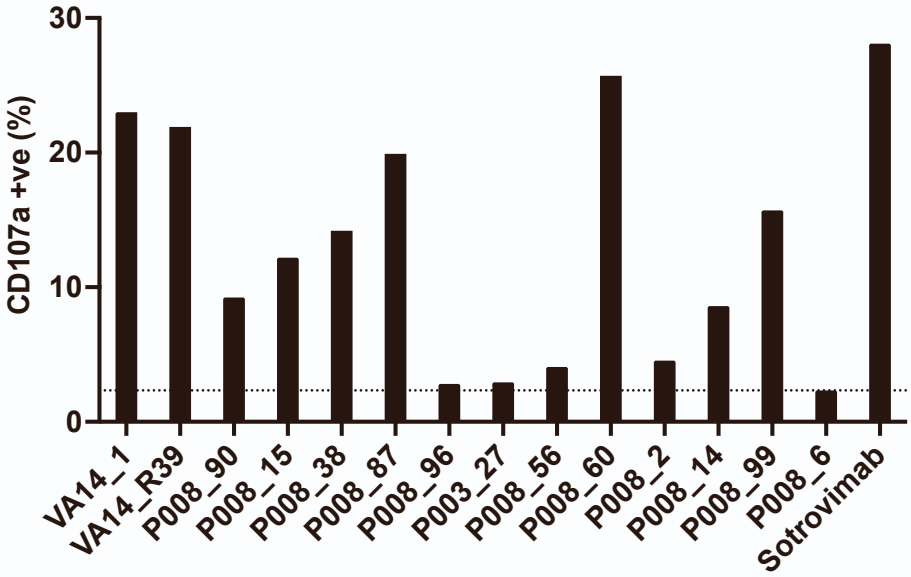

Supplementary Figure S4 – **(A)** Panel of monoclonal antibodies against WT spike, showing their epitope of either Receptor Binding Domain (RBD), N-terminal Domain (NTD), or non-S1 regions; competition group (ND=not done), equivalent antibody class (if an RBD targeting antibody) and the WT spike ELISA EC50 and WT SARS-CoV-2 Pseudovirus Neutralisation IC50. **(B)** ADCC assay measuring activation of NK cells by surface expression of CD107a against same panel of monoclonal antibodies, with the highest degranulation effect plotted here after a 5-fold serial dilution of each monoclonal, starting at 100µg/ml. Related to Fig. 4.

Supplementary Figure S5

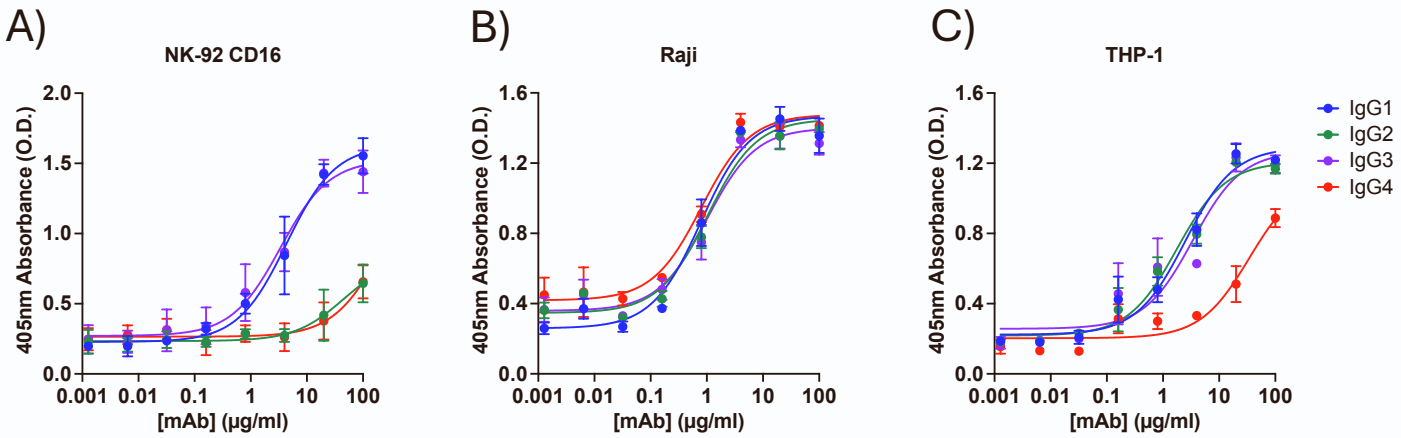

Supplementary Figure S5 – Binding of **i**mmune complexes formed pooled monoclonal IgG1 (blue), IgG2 (green), IgG3 (purple), and IgG4 (red) incubated with recombinant WT Spike, on NK cells **(A)**, Raji cells **(B)**, and differentiated THP-1 cells **(C)**. Data is from 3 biological replicates, plotting geometric mean and standard deviation, and representative of 2 technical replicates. Related to Fig. 4.

Supplementary Figure S6

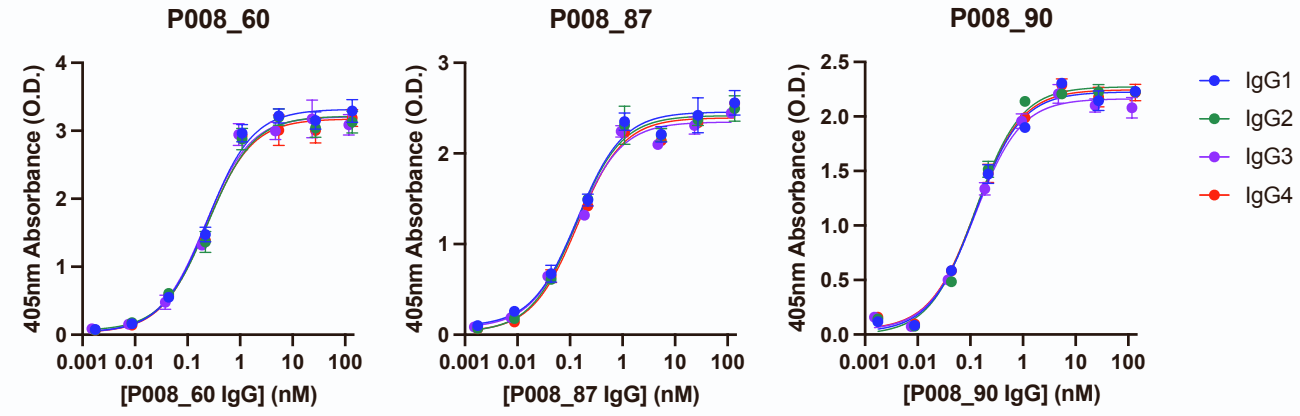

Isotype	EC50 (nM)
IgG1	0.2369
IgG2	0.2436
IgG3	0.2174
IgG4	0.2286

Isotype	EC50 (nM)
IgG1	0.1378
IgG2	0.1301
IgG3	0.1307
IgG4	0.1396

Isotype	EC50 (nM)
IgG1	0.1254
IgG2	0.1241
IgG3	0.1232
IgG4	0.1269

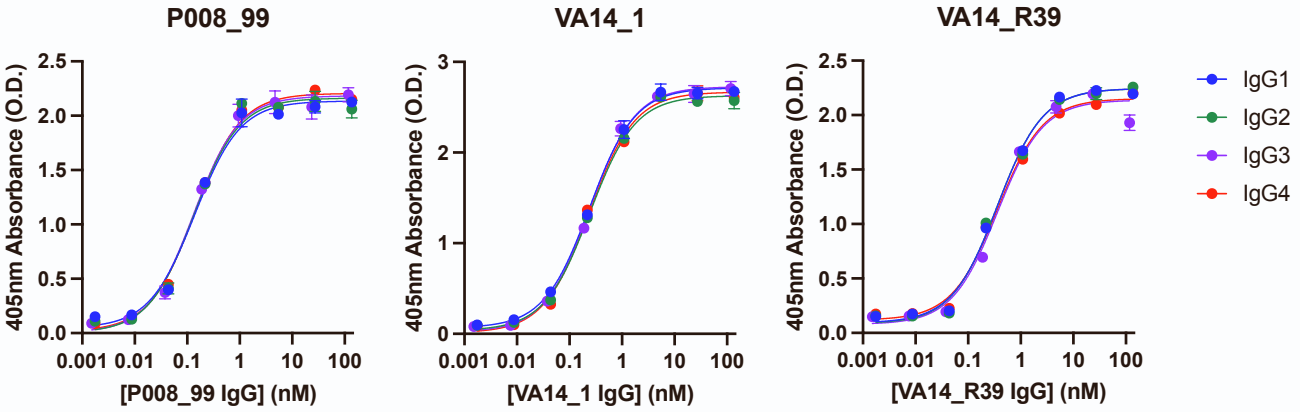

Isotype	EC50 (nM)
IgG1	0.1395
IgG2	0.1333
IgG3	0.1323
IgG4	0.1401

Isotype	EC50 (nM)
IgG1	0.2403
IgG2	0.2431
IgG3	0.2396
IgG4	0.2378

Isotype	EC50 (nM)
IgG1	0.3629
IgG2	0.3588
IgG3	0.3613
IgG4	0.3613

Supplementary Figure S6 – Spike-binding ELISA of monoclonal antibodies P008_60, P008_87, P008_90, P008_99, VA14_1 and VA14_R39, expressed as IgG1 (blue), IgG2 (green), IgG3 (purple), and IgG4 (red), with detection using the same anti-total IgG antibody. EC50 values calculated with Graphpad Prism. Data is from 3 biological replicates, plotting geometric mean and standard deviation, and representative of 2 technical replicates. Related to Fig. 4.

Supplementary Figure S7

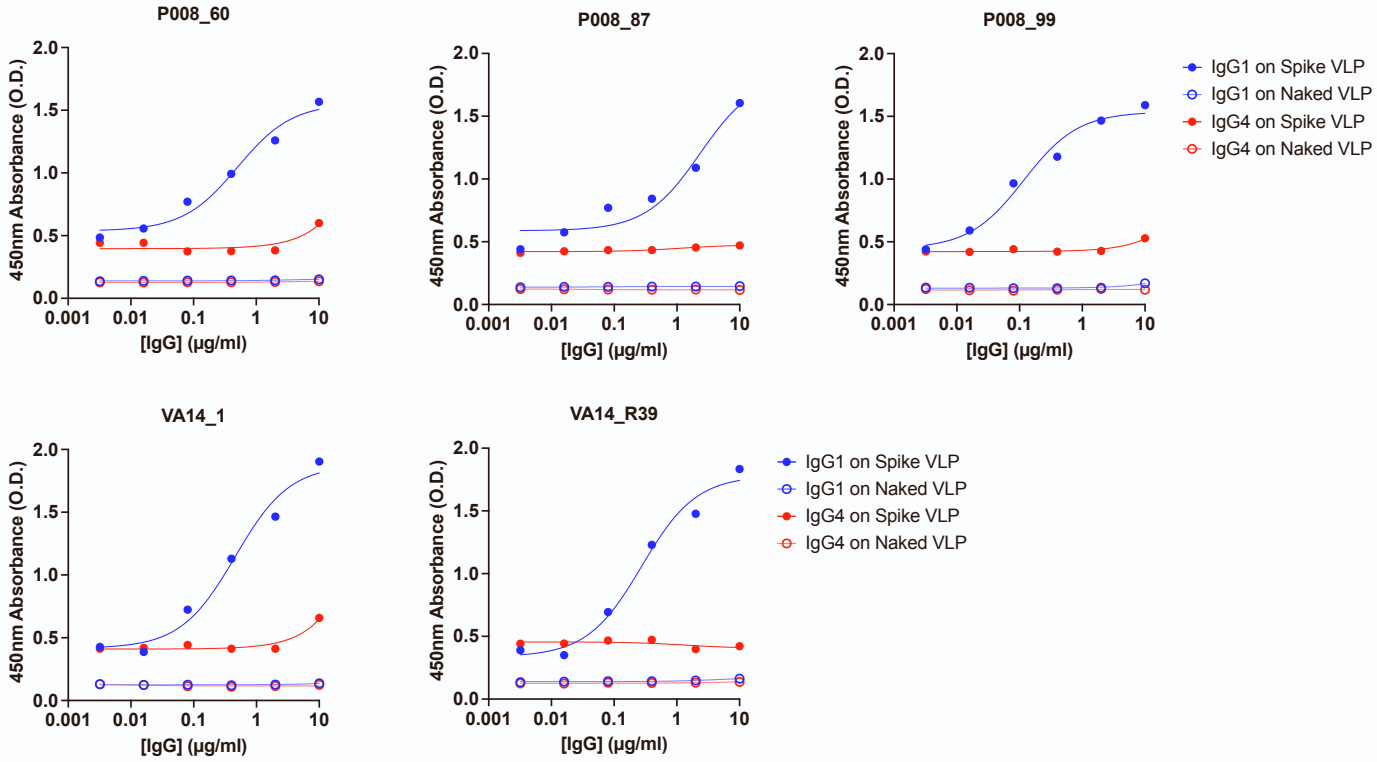

Supplementary Figure S7 – ADCD assay, measuring Complement C3 deposition stimulated by monoclonal IgG1 (blue) or IgG4 (red), against WT Spike Virus-like Particles (VLP) (filled circles) or Naked VLPs (clear circles). Related to Fig 4.

Supplementary Figure S8

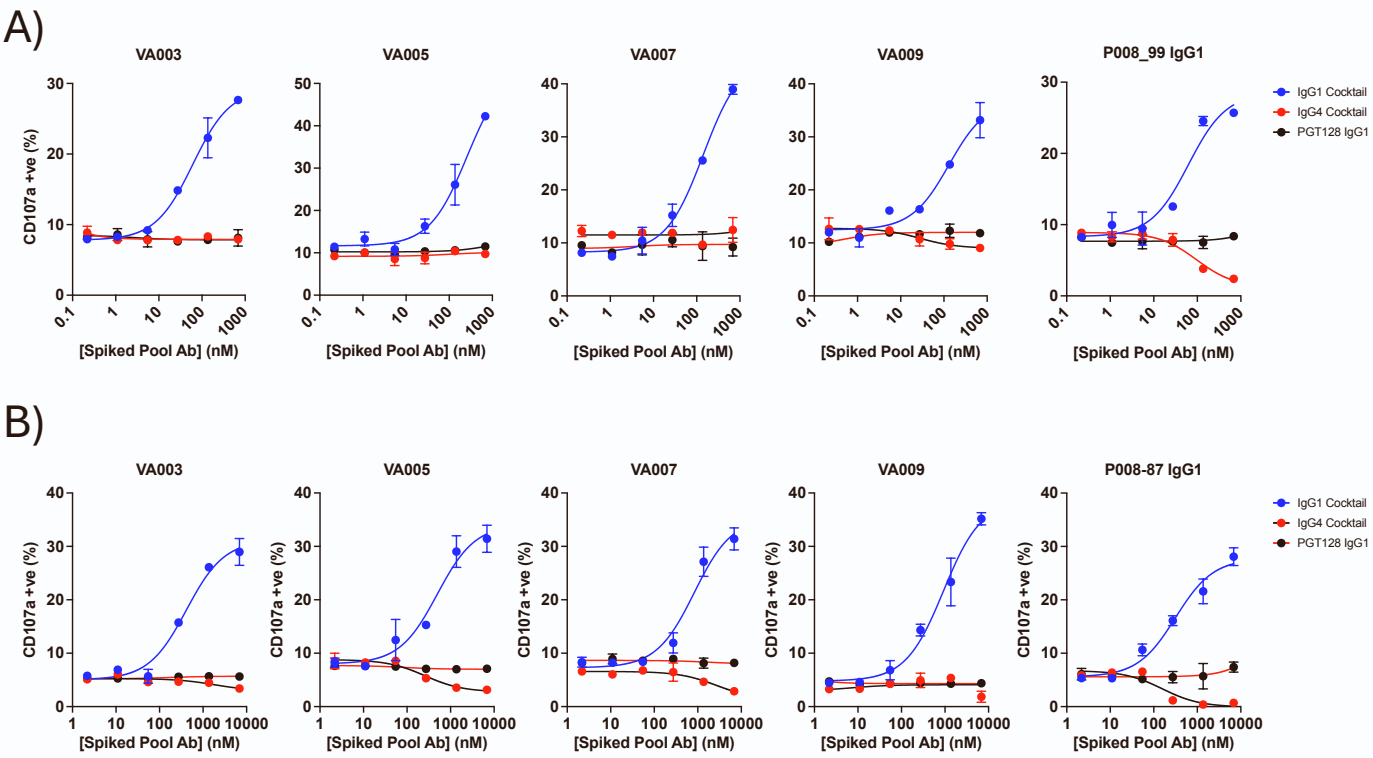

Supplementary Figure S8 – (**A**) ADCC competition assay against SARS-CoV-2 Full Spike, spiking in addition Pooled IgG1 or IgG4 monoclonals (P008_60, P008_87, P008_90, P008_99, VA14_1 and VA14_R39) or IgG1 Isotype Control antibody (anti-HIV IgG1 mAb PGT128) into 4 volunteer plasma samples (Extended Group Post3 samples) at 1:100 dilution or position control of P008_99 IgG1 monoclonal at 1µg/ml. Data is from 2 biological replicates, plotting geometric mean and standard deviation. (**B**) ADCC competition assay against SARS-CoV-2 Receptor Binding Domain only, spiking in additional Pooled IgG1 or IgG4 monoclonals (P008_87, P008_90, VA14_1 and VA14_R39) or IgG1 Isotype Control antibody (anti-HIV IgG1 mAb PGT128) into 4 volunteer plasma samples (Extended Group Post3 samples) at 1:100 dilution or positive control of P008_87 IgG1 monoclonal at 1µg/ml. Data is from 3 biological replicates, plotting geometric mean and standard deviation. Related to Fig. 5.

Supplementary Figure S9

A) Full Spike ADCC

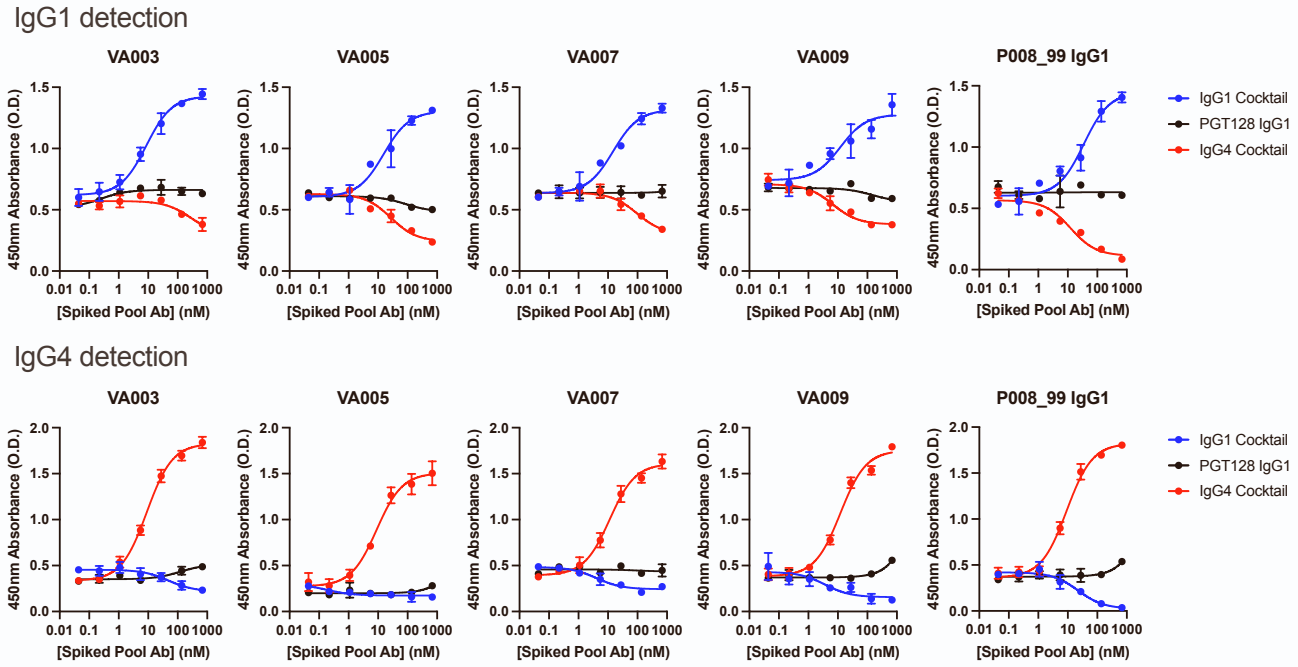

B) RBD ADCC

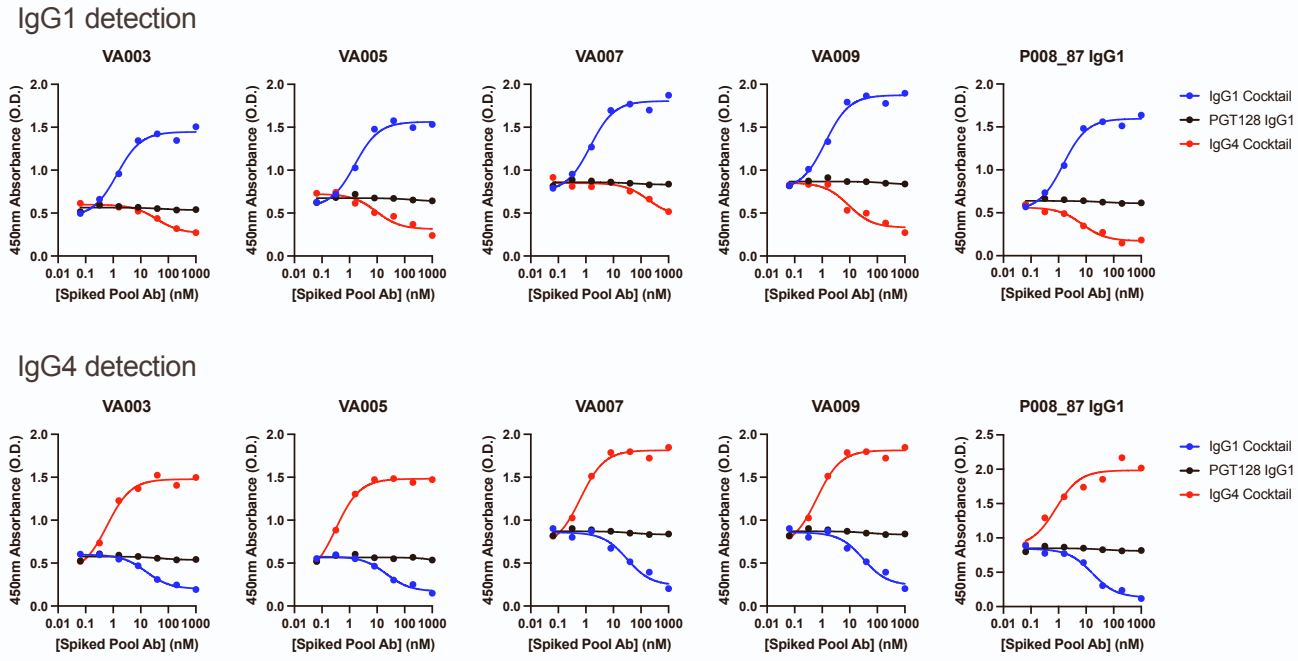

Supplementary Figure S9 – **(A)** Parallel Spike ELISA to Spike Competition ADCC assay, spiking in additional Pooled IgG1 or IgG4 monoclonals (P008_60, P008_87, P008_90, P008_99, VA14_1 and VA14_R39) or IgG1 Isotype Control antibody (anti-HIV IgG1 mAb PGT128) into 4 volunteer plasma samples (Extended Group Post3 samples) at 1:100 dilution or positive control of P008_99 IgG1 monoclonal at 1µg/ml. (**B**) Parallel SARS-CoV-2 WT RBD ELISA to RBD competition ADCC assay, spiking in additional Pooled IgG1 or IgG4 monoclonals (P008_87, P008_90, VA14_1 and VA14_R39) or IgG1 Isotype Control antibody (anti-HIV IgG1 mAb PGT128) into 4 volunteer plasma samples (Extended Group Post3 samples) at 1:100 dilution or positive control of P008_87 IgG1 monoclonal at 1µg/ml. Related to Fig 5.